Data Assimilation and Uncertainty Quantification with Reduced-order Models

by

Zhimin Wu

A Dissertation Presented in Partial Fulfillment
of the Requirements for the Degree
Doctor of Philosophy

Approved November 2021 by the
Graduate Supervisory Committee:

Eric Kostelich, Co-Chair
Mohamed Moustaoui, Co-Chair
Chris Jones
Malena Espanol
Rodrigo Platte

ARIZONA STATE UNIVERSITY

December 2021

ABSTRACT

High-dimensional systems are difficult to model and predict. The underlying mechanisms of such systems are too complex to be fully understood with limited theoretical knowledge and/or physical measurements. Nevertheless, redcued-order models have been widely used to study high-dimensional systems, because they are practical and efficient to develop and implement. Although model errors (biases) are inevitable for reduced-order models, these models can still be proven useful to develop real-world applications. Evaluation and validation for idealized models are indispensable to serve the mission of developing useful applications.

Data assimilation and uncertainty quantification can provide a way to assess the performance of a reduced-order model. Real data and a dynamical model are combined together in a data assimilation framework to generate corrected model forecasts of a system. Uncertainties in model forecasts and observations are also quantified in a data assimilation cycle to provide optimal updates that are representative of the real dynamics. In this research, data assimilation is applied to assess the performance of two reduced-order models.

The first model is developed for predicting prostate cancer treatment response under intermittent androgen suppression therapy. A sequential data assimilation scheme, the ensemble Kalman filter (EnKF), is used to quantify uncertainties in model predictions using clinical data of individual patients provided by Vancouver Prostate Center. The second model is developed to study what causes the changes of the state of stratospheric polar vortex. Two data assimilation schemes: EnKF and ES-MDA (ensemble smoother with multiple data assimilation), are used to validate the qualitative properties of the model using ECMWF (European Center for Medium-Range Weather Forecasts) reanalysis data. In both studies, the reduced-order model is able to reproduce the data patterns and provide insights to understand the underlying

mechanism. However, significant model errors are also diagnosed for both models from the results of data assimilation schemes, which suggests specific improvements of the reduced-order models.

To God, whose love never fails

ACKNOWLEDGMENTS

This dissertation wouldn't be possible without the generous support of many. I first would like to thank my Ph.D. co-advisor Dr. Eric Kostelich, who is a role model in my math career. Dr. Kostelich (or Coach K), you are not only a brilliant applied mathematician but also a genuinely good human being. Thank you for always believing in me (even when I did not believe in myself) and helping me recognize my potential. Your article *Symphony in Chaos* (Kostelich (1995)) and your beautiful work with Chaos theory were what inspired me to come to ASU in the first place. Ever since then, you have always reminded me that there is hope for the future regardless of the challenges that lie ahead. Thank you for teaching me how to apply math to bring good to the world.

I would also like to acknowledge my other co-advisor Dr. Mohamed Moustaoui. Thank you for showing me your passion in atmospheric science and patiently teaching me your knowledge and skills. You have piqued my interest in a new scientific field that I never would've otherwise explored.

Dr. Chris K.R.T. Jones, although you are a remote committee member, you have supported me unconditionally ever since I joined MCRN (Mathematics Climate Research Network). Thank you for being a good listener and always having my best interest in mind. Thank you also for organizing and running MCRN, a highly collaborative national research program that brings many good opportunities to the younger generation of scientists.

I am especially grateful for all the outstanding woman mathematicians who have mentored me along my Ph.D. journey. Dr. Suzanne Lenhart, thank you for seeing my potential during my undergraduate research experience at NIMBios (National Institute for Mathematical and Biological Synthesis) and for encouraging me to pursue a Ph.D in Applied Math, which began a new life trajectory for me. Dr. Malena

Espanol, thank you for actively giving/forwarding me good opportunities to build up my career. My college advisor Dr. Rebekah Yates, I am so fortunate to have you as my first Calculus professor; you helped me discover my love and passion for math through many life-giving conversations in your office.

I am also grateful to connect and work with many talented and supportive graduate students during my study. I appreciate learning from each of my collaborators through MCRN: Julie Sherman, Ligia Flores, Kiara Sanchez, and Yorkinoy Shermatova. I would also like to thank my friends and colleagues at ASU, Dr. Elpiniki Nikolopoulou, Dr. Lauren Johnson, Dr. Tin Phan, and Duane Harris.

Last but not least, I could never have persevered through such a difficult time during the pandemic without the selfless love from my friends and family. Thank you to my mom and dad, Shuiqiong Zhang and Wanhong Wu, for standing by me whenever I needed you from another side of the ocean. Thank you to my church family, Symphony Church in Boston, for all your prayers for me. Thank you to my American family, the Gartmans: Julia, Dee, and Keith, for all your unconditional love and for adopting me (unofficially) into your family since my college days. Thank you also to my dear friends in China, Shuixin Zhong and Zhilin Wu, for always accompanying me during my sleepless nights.

The research of this dissertation was supported by a grant to Eric Kostelich and Yang Kuang by the Arizona Biomedical Research Commission, and the National Science Foundation funding of the MCRN through a grant to the American Institute of Mathematics.

TABLE OF CONTENTS

CHAPTER Page

CHAPTER Page

LIST OF TABLES

LIST OF FIGURES

Figure Page

Chapter 1

INTRODUCTION

Developing mathematical models for high-dimensional dynamical systems can be challenging because of the complexity of underlying mechanisms. For example, it is difficult to achieve high accuracy in modeling the global dynamics of atmospheric weather due to a large system state that includes the physics and chemistry occurring in the atmosphere. Developing such a high-dimensional model can be costly in both intellectual effort and computational power. In most real-world applications, we do not have the required knowledge or computing system to develop and simulate a high-dimensional dynamical model. Alternatively, reduced-order modeling is often used to study complex high-dimensional systems. It simplifies a high-dimensional dynamical system by reducing the system's state dimension significantly without losing the fundamental mechanism of the observed system. Although reduced-order models are idealized representations of the respective realities, it is proven efficient and practical to simulate and study the main causes of a high-dimensional system. In this thesis, I will present applications of reduced-order modeling in both mathematical medicine and climate.

For the first project, I use an ODE (ordinary differential equation) model to study the growth of a prostate tumor undergoing the intermittent androgen suppression (IAS) therapy. Due to limited clinical measurements of the prostate tumor, I am only able to use a time series of blood serum prostate specific antigen (PSA) level to approximate the tumor growth. Hence, the mathematical model simplifies the change of tumor volume to a one-dimensional system represented by the PSA level at different times of a treatment journey. For the second project, I am interested in studying the

change of state of the stratospheric polar vortex. Since it is computationally expensive to simulate a global model to study the long-term dynamics of the polar vortex, I use three ordinary differential equations that localize the polar vortex to a single point in the stratosphere to model the stratospheric wind-wave interactions.

In both studies, a reduced-order model is obtained to approximate the true dynamics due to limited measurements (data) and theoretical knowledge to fully understand its underlying mechanisms. Reduced-order modeling ignores the unknowns of a complex dynamical system and focuses only on what is known at the current stage. Furthermore, real data are used to compare with model forecasts in order to verify and update corresponding model assumptions. The ultimate goal of using reduced-order models for both projects is to capture the main causes of the observed system and recover the qualitative behaviors of the system. The model of prostate cancer treatment is used to foretell if and how much the cancer cell population will decrease after a patient receives treatment, which can inform the patient and doctor if the treatment will be effective. Similarly, the reduced-order model of the Arctic polar vortex describes the annual and inter-annual variations of the polar vortex, which can be used to interpret a warm or cold winter in the Northern Hemisphere. These reduced-order models can be used to build useful applications to answer interested scientific questions.

Although reduced-order models are much easier to develop and implement than high-dimensional models, they suffer from consequential uncertainty because of simplification of realities. Many aspects of a dynamical system are ignored in the development of a reduced-order model. Hence, it is necessary to assess the reliability and/or predictability of idealized models. "All models are wrong, but some are useful" is a well-known quote by a late British statistician, George Box (Box (1976)). This states my motivation to assess and validate the performances of reduced-order

models for the two projects. I acknowledge that these idealized models are limited to explain everything one can observe about the interested systems, but these simple models can still be used to answer certain important scientific questions if it can be proven that the model performance is representative of the observed reality.

Data assimilation is one popular way to assess a dynamical model's performance. It is a procedure that combines a dynamical model with available observations of the system and produces updated analysis of the model's state. Meanwhile, data assimilation also provides statistics for observation errors and model errors (biases) in its updates. Generally, two steps are involved in a data assimilation scheme: a background forecast (prior estimate of the system state) and an analysis cycle (posterior estimate of the system state). The background forecast (or background) is the initial guess of the system state, so it serves as the initial condition(s) of the dynamical model. The background is used to simulate the model in a short time scale until new observations are available for the dynamical system. Then, the analysis cycle is generated by combining the new observations with the current background to produce an updated (corrected) initial guess of the system state. The analysis serves as the new initial guess (background) for the next data assimilation cycle and the previous procedure repeats. One optimal analysis cycle would achieve good "synchronization" between the physical system (observation space) and the model state. Data assimilation is an iterative approach alternating between the background forecast and analysis cycle, and it keeps track of the uncertainty of model predictions in real time.

Figure 1.1 shows a simple example of data assimilation applied to estimate the temperature at a location. The orange circles represent the background forecasts from a model at different times, the blue stars are real observations, and the red squares are the analysis cycles generated by the data assimilation algorithm. At each time

point when there is an observation available, the analysis is generated by combining two pieces of information: the background forecast and an observation, to produce a more accurate estimate of the temperature, which is the analysis. Ideally, the analysis should improve the model predictions as shown in this figure that it is closer to the true temperature (blue curve) than the original forecast. Moreover, the two-step procedure of data assimilation is repeated every time when a new observation becomes available. Thus, data assimilation is an iterative approach.

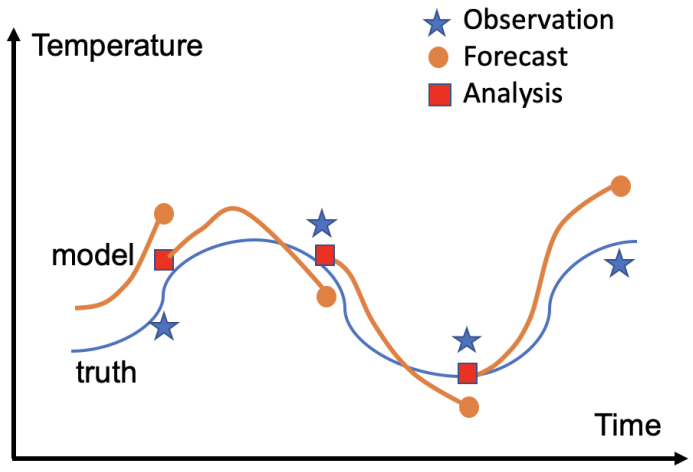

Figure 1.1: An example of data assimilation applied to predict the future temperature at a location. The two-step data assimilation cycle is repeated whenever a new observation is available.

A major challenge in the projects described here is that the provided data (observations) are inadequate to estimate some important model parameters. For example, the model for prostate cancer treatment has 21 parameters in total. However, only two types of clinical measurements are available for individual patients: blood serum androgen and PSA level. These two time series do not provide enough information to estimate each parameter correctly for an individual patient. If truthful param-

eter values are not provided for each patient, then the parameter space will also contribute to the uncertainty of model predictions and jeopardize the reliability of short-term predictions. Similar issues also remain for the polar vortex project. There are two control parameters of the model that represent the physical perturbations to the stratospheric polar vortex, but no direct observations are available to estimate those control parameters. The reduced-order model requires control parameters that are consistent with observed data to reproduce the observed dynamics. Hence, for both projects I realized that quantifying uncertainty only for the model state does not guarantee that the models produce reasonable forecasts.

To cope with the uncertainty associated with parameter space, I have decided to include parameter estimation as a part of a data assimilation scheme. For both projects I have chosen some important model parameters and used data assimilation algorithms to estimate those parameters directly from given data sets. This parameter-estimation procedure can be seen as solving an inverse problem because the data are used to infer the correct values of chosen model parameters.

For the prostate cancer treatment project, I have designed an augmented state vector that includes both the model state vector and a vector for chosen model parameters. A new dynamical model is also developed for the augmented state vector, which is implemented within the ensemble Kalman filter (EnKF) framework. The EnKF is a sequential data assimilation scheme that updates both the model state and the parameter space simultaneously. The mean of ensemble forecasts is used to represent the final estimate for the system state.

For the polar vortex project, I have chosen two different data assimilation schemes to estimate a control parameter of the reduced-order model under different assumptions. The first approach is the same design as the prostate cancer treatment project – using EnKF with an augmented state vector. The second approach is a global data

assimilation scheme called the ensemble smoother with multiple data assimilation (ES-MDA). The ES-MDA only updates the parameter space so that the model with estimated parameters can be used to reproduce the entire historical data set. More details about the assumptions for different data assimilation schemes will be given in Chapter 5 and 6. The overall goal for this dissertation is to demonstrate the efficiency of reduced-order modeling to study high-dimensional systems and how to assess and validate these idealized models using data assimilation.

1.1 Background of Data Assimilation

Data assimilation was first developed to aid with numerical weather prediction (NWP). NWP can be viewed as an initial value problem: given an estimate of the current state of the atmosphere (initial conditions), we want to obtain short-range forecasts of the atmospheric evolution. In the early developments of NWP, interpolations of the available observations to a regular grid were performed manually to provide initial conditions for a forecast model. Jule Charney first envisioned in his 1951 paper (Charney (1951)) that an automatic "objective analysis" of meteorological data was much needed to replace the time-consuming hand analyses. Now we refer to this automated procedure as data assimilation, which combines observations with short-range forecasts to estimate the initial conditions. As described in Talagrand (1997), the purpose of data assimilation is "using all the available information, to determine as accurately as possible the state of the atmospheric (or oceanic) flow."

One important problem to be considered for determination of atmospheric state is: current observations alone are not enough to initialize a forecast model. Modern forecast models can have a state dimension of the order of 10^7, whereas the total number of conventional observations for the corresponding model variables is of the order of 10^4 (Kalnay (2003)). Moreover, the distribution of these data is very nonuniform

in time and space. Regions such as the North America and Eurasia are much more densely observed than the oceans. Due to the inadequacy of observations, additional information needs to be used to complete the initial guess of atmospheric state. We also refer to the initial guess as the background or prior information.

Data assimilation updates (improves) the background whenever new data become available, which is known as the "analysis cycle". The analysis cycle provides a forecast model corrected initial conditions based on the new information and hence improves short-range forecasts. The short-range forecast then is used as the first guess (background) for the next analysis cycle and so on. Currently, the intermittent data assimilation cycle is performed every 6 hours and four times a day in operational global forecast models. In each data assimilation cycle, all available new observations and physical laws that govern the flow are used to update the initial conditions. This approach not only provides a complete initialization of the global grid but also carries information from the data-rich regions to the data-poor regions. For example, a data-poor region like the North Atlantic Ocean could still have a good forecast benefiting from the upstream information carried from the data-rich region North America.

The performance of a data assimilation cycle is significantly affected by the choice of analysis schemes. There are two major categories of analysis schemes: empirical schemes and statistical interpolation schemes. Successive corrections method (SCM) is the first empirical analysis scheme developed by Bergthörsson and Döös (1955) and by Cressman (1959). Newtonian relaxation (or nudging) is another empirical scheme developed later in the 1970s by Hoke and Anthes (1976) and by Kistler (1974). The empirical methods are simple but limited for large-scale assimilation. Instead, the statistical interpolation schemes, in particular least squares methods, are more widely used in current global operational forecasts. Some popular statistical interpolation schemes are Kalman filtering (KF), 3D-Var and 4D-Var assimilation. There are many

good literature reviews of detailed discussions for different analysis schemes developed over the decades. Articles from Ghil and Malanotte-Rizzoli (1991), and Talagrand (1997) give a rigorous overview of current methods of data assimilation. There are also books by Bengtsson *et al.* (1981), Daley (1993) and Kalnay (2003) that contain a comprehensive description of methods for atmospheric data assimilation.

Although the designs of various data assimilation analysis schemes look very different from each other, they all share the same goal of quantifying observation errors and model (forecast) errors in the background to optimize the analysis cycles. Empirical schemes use arbitrary tuning parameters to approximate such errors, and statistical interpolation schemes use error statistics such as the covariance matrix to quantify the background uncertainty. Generally, it is important to capture the errors in both observations and the background efficiently to obtain short-range forecasts that are close to the real atmosphere.

In addition to considering the errors introduced by observations and model deficiencies in data assimilation cycles, the chaotic nature of atmospheric flows discovered by Edward Lorenz suggested another major improvement for NWP: ensemble forecasting (Lorenz (1965)). Lorenz pointed out that due to the instabilities of atmospheric flows, any small errors (either from the model or initial conditions) could grow quickly over time and reduce the accuracy of forecast models dramatically. He estimated the limit of weather predictability as about two weeks. This finding encouraged the replacement of single deterministic forecast to an ensemble forecast with different initial conditions to represent the stochastic nature of atmospheric evolution. In this dissertation, we focus only on ensemble methods to develop respective real-world applications.

1.2 Data Assimilation for Reduced-order Modeling

Although data assimilation was initially developed for operational NWP to solve the initial value problem for atmospheric predictions, many principles of its design are still practical and transferable to other domains of science. As described briefly in the above section, data assimilation is an iterative algorithm of two steps: background and analysis. This two-step structure is ideal for dynamical systems that have incomplete observations for the state space and need additional information to update initial conditions. Data assimilation provides optimal updates for the current state of a system by combining available observations with model forecasts. In addition, the analysis cycle also considers errors from observations and model forecast (or the background) to update the initial conditions iteratively so that the updated short-range forecast is close to the real dynamics. Lastly, the option of ensemble forecasting in data assimilation provides reliable predictions for chaotic dynamical systems that are sensitive to errors in initial conditions.

Data assimilation has been proven robust in forecasting high-dimensional systems since its first development in the 1950s, and it still contributes to many operational global forecast models today. For example, the European Center for Medium-Range Weather Forecasts (ECMWF) incorporates data assimilation into its global forecast models and provides archives of hourly estimates of atmospheric and oceanic climate variables, which is known as the ECMWF Reanalysis data.

The challenges that have been overcome for NWP can also be found in many applications for reduced-order modeling. Often reduced-order models are used to simplify a complex high-dimensional system to better understand the underlying mechanism. As a result of the simplification, there is always inevitable model error in the model's simulation (prediction) of respective reality. Moreover, in most real-world applica-

tions, a reduced-order model is built after the observations are collected. Hence, most of the model variables lack real observations to be initialized or validated. Reduced-order modeling shares the same issue of initial condition uncertainty as NWP. In order to assess and validate reduced-order models, quantifying errors caused by model deficiency and incomplete data is necessary as well. Therefore, the design of data assimilation is much applicable to resolve similar challenges encountered in reduced-order modeling.

In recent years, data assimilation has been applied in some other domains of social and physical sciences. Evensen *et al.* (2020) adapted data assimilation to a low-dimensional disease model to study the spread of COVID-19 over different regions of the world. Similarly in my study, I have adapted various data assimilation methods to develop applications for mathematical medicine and climate.

The first project is about developing a predictive model for prostate cancer treatment response. The second project is about developing a mechanistic model to understand what causes the changes in the state of polar vortex in the Northern Hemisphere. For both projects, the models are low-dimensional models of ordinary differential equations built upon assumptions of underlying mechanisms. These models focus majorly on studying the qualitative behaviors of corresponding dynamical systems. For example, the polar vortex model assumes inter-annual variability of stratospheric polar vortex: some winters the polar vortex is stable and associated with high zonal wind speed, whereas other winters an unstable polar vortex is observed with low zonal wind speed. High quality data are obtained to test relevant model assumptions and thus validate the model performance. Data assimilation is applied in both projects to combine the mathematical model with real data, subsequently, it provides a computational model for the dynamical system. Moreover, the developed data assimilation framework is also able to estimate important model parameters directly so that the

model is calibrated in real time to produce short forecasts that are representative of reality.

The data assimilation framework is developed to answer different scientific questions for the two projects. The prostate cancer project focuses on the predictive ability of a mathematical model. A common problem discovered for prostate cancer models is that parameters that provide good fits to previous data do not assure accurate predictions for the future. Hence, the developed data assimilation framework aims to quantify (correct) errors in model forecasts to ensure the model's prediction accuracy. On the other hand, the polar vortex project is more concerned with the representativeness of a low-dimensional model that is used to study the mechanism of the Arctic polar vortex. The model presented in my study is a crude reduction of the high-dimensional system of stratospheric polar vortex. Consequently, model bias is inevitable for such a low-dimensional mechanistic model of the polar vortex. In this case, the developed data assimilation framework is used to identify potential model bias and to verify the model's representativeness of reality. It is discovered that an accurate parameter estimation is essential to reproduce the observed dynamical system. More detailed discussions of the results of both projects will be provided in Chapter 4 and 6, respectively.

The structure of this dissertation is as follows. Chapter 2 introduces the conceptual formulation of data assimilation methods used in this dissertation. Chapter 3 presents the background information and mathematical modeling for prostate cancer treatment. Chapter 4 describes the data assimilation applications for prostate cancer treatment response prediction. This result is published in the journal *Mathematical Biosciences and Engineering*. Chapter 5 introduces a low-dimensional model of the Arctic polar vortex. Chapter 6 presents the data assimilation applications for the reduced-order model of the polar vortex.

Chapter 2

DATA ASSIMILATION

As mentioned briefly in Chapter 1, data assimilation solves an initial value problem for a dynamical system by combining the current background forecast with available observations. The background forecast is obtained by integration of a dynamical model with given initial conditions. In the context of numerical weather prediction, the dynamical model is a high-dimensional model that describes the physical laws governing the atmospheric and oceanic flows. However, in this thesis, the models developed for the two projects are both reduced-order models, which are given by a set of ordinary differential equations in the form

$$\frac{d\mathbf{x}}{dt} = F(t, \mathbf{x}), \tag{2.1}$$

where $\mathbf{x}$ is an m-dimensional state vector representing the system state at a given time.

A data assimilation cycle is constructed with these two steps: forecast and analysis, denoted as $\mathbf{x}^b$ and $\mathbf{x}^a$, respectively. The forecast can also be called background, first guess or prior information. The background is given by integrating the model in Equation (2.1) with given initial conditions of the state vector. The main goal of data assimilation is to calculate an "optimal" update for current background using new observations $\mathbf{y}^o$ (a vector of observed model variables), which produces the analysis. An observation operator is required in this process to map model variables to the observation space, which is denoted as H. The difference between the observations and the model first guess $\mathbf{y}^o - H(\mathbf{x}^b)$ is called observational increments or "innovations". The analysis is given by adding the innovations to the background

forecast with weights $\mathbf{W}$ that are calculated based on statistical error covariances of the forecast and the observations, defined as

$$\mathbf{x}^a = \mathbf{x}^b + \mathbf{W}\left[\mathbf{y}^o - \mathbf{H}(\mathbf{x}^b)\right]. \tag{2.2}$$

Different analysis schemes can be used to determine the weights $\mathbf{W}$. There are both empirical methods such as successive corrections method (SCM) (Bergthörsson and Döös (1955); Cressman (1959); Barnes (1964)) and statistical interpolation methods such as Kalman filtering (KF) (Kalman (1960); Kalman and Bucy (1961)) and 3D-Var (Sasaki (1970)) to calculate the weights. The analysis schemes used in this thesis are derived from the KF: ensemble Kalman filter (EnKF) and ensemble smoother with multiple data assimilation (ES-MDA). The KF assumes Gaussian distributions to the errors in the background and observations and provides a linear estimate of the "true" system state using the error statistics.

This chapter begins with a simple scalar example of the Kalman filter, and then proceeds to the ensemble-based methods. Practical challenges associated with these methods will be discussed as well.

2.1 Kalman Filtering for a Scalar

The Kalman filter is one of the variational approaches that defines a cost function to determine the weights $\mathbf{W}$ in Equation (2.2). Let us simplify the problem by considering a one-dimensional state variable with one observation available currently.

Suppose an estimate of current room temperature (from thermostat) is given as T_b, and this estimate has some error ϵ_b that is assumed to have a Gaussian distribution with mean 0 and variance σ_b^2. Then a thermometer is used to measure current room temperature which gives an observation T_o associated with an error ϵ_o assumed to have a Gaussian distribution with mean 0 and variance σ_o^2. The error terms ϵ_b and ϵ_o are assumed to be independent from each other. The problem needs to be solved

here is to recover the most likely value of the true temperature T based on the two noisy estimates. Basically, this is solving the analysis (Equation (2.2)) in the scalar form

$$T_a = T_b + W(T_o - T_b), \tag{2.3}$$

where the observation operator H becomes the identity and the analysis T_a serves as the "most likely value of true temperature".

The probability distribution (PDF) of the estimate T_b given a true value T and a Gaussian error with variance σ_b^2 is given by the Gaussian distribution

$$p(T_b|T) = \frac{1}{\sqrt{2\pi}\sigma_b} e^{-(T_b-T)^2/(2\sigma_b^2)}. \tag{2.4}$$

Similarly, the PDF of the estimate T_o given a true value T and a Gaussian error with variance σ_o^2 is given by the Gaussian distribution

$$p(T_o|T) = \frac{1}{\sqrt{2\pi}\sigma_o} e^{-(T_o-T)^2/(2\sigma_o^2)}. \tag{2.5}$$

These two PDFs are also called the likelihood of a true value T given the corresponding estimates.

Since T_b and T_o are independent, the most likely value of T is the one that maximizes the joint probability

$$p(T|T_b, T_o) = p(T_b|T)p(T_o|T) = \frac{1}{2\pi\sigma_b\sigma_o} e^{-\frac{(T_b-T)^2}{2\sigma_b^2} - \frac{(T_o-T)^2}{2\sigma_o^2}}. \tag{2.6}$$

Maximizing the exponential function is equivalent to minimizing the cost function

$$J(T) = \frac{1}{2}\left[\frac{(T_b - T)^2}{\sigma_b^2} + \frac{(T_o - T)^2}{\sigma_o^2}\right]. \tag{2.7}$$

Expanding the quadratic expressions for Equation (2.7) and completing the square gives

$$J(T) = \left(\frac{1}{\sigma_b^2} + \frac{1}{\sigma_o^2}\right)\left[T - \frac{\sigma_o^2 T_b + \sigma_b^2 T_o}{\sigma_o^2 + \sigma_b^2}\right]^2 + C, \tag{2.8}$$

where C is constant with respect to T. Thus, the minimizer or the analysis of $J(T)$ is given by

$$T_a = \frac{\sigma_o^2 T_b + \sigma_b^2 T_o}{\sigma_o^2 + \sigma_b^2}. \tag{2.9}$$

Notice that one could also set the first derivative of $J(T)$ equal to zero and solves for T to obtain the same results. Here, we set Equation (2.9) equal to Equation (2.3) and solve for W which gives the optimal weight as

$$W = \frac{\sigma_b^2}{\sigma_b^2 + \sigma_o^2}, \tag{2.10}$$

which is also referred to as the "Kalman gain". Equation (2.8) also gives the analysis error variance as

$$\frac{1}{\sigma_a^2} = \frac{1}{\sigma_b^2} + \frac{1}{\sigma_o^2} = \frac{\sigma_b^2 + \sigma_o^2}{\sigma_b^2 \sigma_o^2}, \tag{2.11}$$

or

$$\sigma_a^2 = (1 - W)\sigma_b^2. \tag{2.12}$$

This analysis gives an intuitive understanding of how the filter works: if the observation error σ_o^2 is large, then $W \ll 1$ and $\sigma_a^2 \approx \sigma_b^2$, so the filter gives more weight to the background forecast. Similarly, if the background error σ_b^2 is large, then $W \approx 1$ and $\sigma_a^2 \approx \sigma_o^2$, so the filter will give much more weight to the measurement given by the thermometer.

2.2 Multi-dimensional Case of the Kalman Filter

Now let us go back to the multi-dimensional system defined in Equation (2.1). Suppose $\mathbf{x}^b \in \mathbb{R}^m$ is the current background state vector and $\mathbf{y}^o$ is an l-dimensional vector of observed model variables ($l \leq m$). They are assumed to have Gaussian errors with uncertainties quantified by covariance matrices $\mathbf{P}^b$ and $\mathbf{R}$, respectively. In particular, the observation vector has the relationship with the true system state

$\mathbf{x}$:

$$\mathbf{y}^o = H(\mathbf{x}) + \epsilon^{\mathbf{o}}, \tag{2.13}$$

where ϵ^o is a Gaussian random variable with mean $\mathbf{0}$ and covariance matrix $\mathbf{R}$. Then, the cost function analogous to Equation (2.7) is given by

$$J(\mathbf{x}) = [\mathbf{x} - \mathbf{x}^b]^T (\mathbf{P}^b)^{-1} [\mathbf{x} - \mathbf{x}^b] + [\mathbf{y}^o - H(\mathbf{x})]^T \mathbf{R}^{-1} [\mathbf{y}^o - H(\mathbf{x})]. \tag{2.14}$$

If the model dynamics and the observation operator are both linear, then there exists a unique minimizer for Equation (2.14), which can be obtained by completing the square similarly to what we did for Equation (2.8). The analysis is given by the state estimate $\mathbf{x}^a$ and its covariance matrix $\mathbf{P}^a$ and needs to satisfy

$$J(\mathbf{x}) = [\mathbf{x} - \mathbf{x}^a]^T (\mathbf{P}^a)^{-1} [\mathbf{x} - \mathbf{x}^a] + C' \tag{2.15}$$

for some constant C'. To solve for $\mathbf{x}^a$ and $\mathbf{P}^a$, we expand Equation (2.14) and equate the terms of degree 2 in $\mathbf{x}$ and we have

$$\mathbf{P}^a = \left[(\mathbf{P}^b)^{-1} + \mathbf{H}^T \mathbf{R}^{-1} \mathbf{H} \right]^{-1}. \tag{2.16}$$

We equate the terms of degree 1 in $\mathbf{x}$ and we have

$$\mathbf{x}^a = \mathbf{P}^a \left[(\mathbf{P}^b)^{-1} \mathbf{x}^b + \mathbf{H}^T \mathbf{R}^{-1} \mathbf{y}^o \right]. \tag{2.17}$$

Equations (2.16) and (2.17) can also be rearranged to the have the following form

$$\mathbf{P}^a = \left[\mathbf{I} + \mathbf{P}^b \mathbf{H}^T \mathbf{R}^{-1} \mathbf{H} \right]^{-1} \mathbf{P}^b \tag{2.18}$$

$$\mathbf{x}^a = \mathbf{x}^b + \mathbf{K} \left(\mathbf{y}^o - \mathbf{H}\mathbf{x}^b \right), \tag{2.19}$$

where $\mathbf{K} = \mathbf{P}^a \mathbf{H}^T \mathbf{R}^{-1}$ is the Kalman gain matrix. Note that $\mathbf{K}$ is the weight matrix in the context of KF. Equations (2.18) and (2.19) are the so called Kalman filter update equations. Notice that a linear combination of Gaussian distributions is still Gaussian, so the updated analysis also has a Gaussian error.

All the computations above are done at the same time point t_n, so we dropped the notation for time to demonstrate how one analysis cycle works. In real practice, the background and analysis are performed sequentially at times $t_1 < t_2 < \cdots < t_n$ when observations become available. The updated analysis serves as the new first guess (background) for the next analysis cycle and the above process repeats. In the case of a linear model, let $\mathbf{M}_{t,t'}$ be the matrix that propagates the solution from time t to t'. The sequential scheme can be written as

$$\mathbf{x}_n^b = \mathbf{M}_{t_{n-1},t_n}\mathbf{x}_{n-1}^a, \tag{2.20}$$

$$\mathbf{P}_n^b = \mathbf{M}_{t_{n-1},t_n}\mathbf{P}_{n-1}^a\mathbf{M}_{t_{n-1},t_n}^T, \tag{2.21}$$

which uses previous step's analysis $\mathbf{x}_{n-1}^a$ and its covariance $\mathbf{P}_{n-1}^a$ to calculate the current time step's analysis update. Then, the current analysis update will be used as the new background for the next iteration of data assimilation cycle.

2.3 Ensemble Kalman Filtering for Nonlinear Scenario

The KF is developed for linear dynamics. In the case that the dynamical model (Equation (2.1)) and the observation operator become nonlinear, the KF fails to update the background uncertainty $\mathbf{P}_n^b$ precisely. The ensemble Kalman filter (EnKF) was originally proposed by Evensen (1994) to solve for nonlinear dynamics. The main concept of the EnKF is to use an ensemble of background estimates at time t_{n-1} and propagate each ensemble member to time t_n and use their spread to characterize the covariance $\mathbf{P}_n^a$.

Here we drop the time notation again for simplicity and denote the background ensemble with size k as $\{\mathbf{x}^{b(i)}\}_{i=1}^k$. The best estimate for the current system state is given by the background ensemble mean

$$\overline{\mathbf{x}}^b = k^{-1}\sum_{i=1}^{k}\mathbf{x}^{b(i)}. \tag{2.22}$$

Then, the sample covariance of the background ensemble is given as

$$\mathbf{P}^b = (k-1)^{-1}\mathbf{X}^b(\mathbf{X}^b)^T, \tag{2.23}$$

where $\mathbf{X}^b$ is the $m \times k$ background perturbation matrix whose ith column is given as $\mathbf{x}^{b(i)} - \overline{\mathbf{x}}^b$. The EnKF produces an analysis ensemble $\{\mathbf{x}^{a(i)}\}_{i=1}^k$ with sample mean and covariance, respectively

$$\overline{\mathbf{x}}^a = k^{-1}\sum_{i=1}^{k}\mathbf{x}^{a(i)}, \tag{2.24}$$

$$\mathbf{P}^a = (k-1)^{-1}\mathbf{X}^a(\mathbf{X}^a)^T, \tag{2.25}$$

where $\mathbf{X}^a$ is the $m \times k$ analysis perturbation matrix whose ith column is given as $\mathbf{x}^{a(i)} - \overline{\mathbf{x}}^a$. The background mean $\overline{\mathbf{x}}^b$ and its associated sample covariance matrix $\mathbf{P}^b$ are used to define the cost function Equation (2.14) which yields the updated analysis ensemble with mean $\overline{\mathbf{x}}^a$ and covariance matrix $\mathbf{P}^a$ that appear in similar forms as Equations (2.18) and (2.19).

The EnKF algorithm also requires a routine to choose a specific analysis ensemble, as there are many possible choices of an analysis ensemble to provide the matrix $\mathbf{X}^a$. The simplest case is to apply the KF update equation, Equation (2.17), directly to each background ensemble member to obtain the corresponding analysis ensemble. However, this method tends to give a sample covariance that is smaller than the analysis covariance given by Equation (2.18). Instead, the ensemble square-root filter (Anderson (2001); Whitaker and Hamill (2002); Tippett *et al.* (2003); Ott *et al.* (2002)) is applied to construct an analysis ensemble with mean and sample variance that are the same as the KF update equations in the linear case as Equations (2.18) and (2.19). Square root filters are also known as a deterministic version of the EnKF (Whitaker and Hamill (2002)), which is different from the earlier approach used in Evensen (1994); Burgers *et al.* (1998); Houtekamer and Mitchell (1998), where ob-

servations are perturbed artificially to generate each analysis ensemble member. The EnKF frameworks developed for the prostate cancer treatment project and the polar vortex project both use the square root filters.

2.3.1 Covariance Inflation

The classical KF update equations stated above produce unbiased system updates only if the covariances $\mathbf{P}^b$ and $\mathbf{P}^a$ are representative of the underlying uncertainties. However, in reality, an accurate estimate for the error covariances can be hindered by many factors. One of the main causes is model error, which is common for nonlinear dynamics. The EnKF tends to underestimate the uncertainty because of model errors (biases), which leads to overconfidence in the background forecasts. Eventually, the data assimilation system ignores the observations and decouples from the true trajectory.

Different *ad hoc* procedures (using tunable parameters for the framework) have been developed to resolve this problem. Generally, one can inflate the estimated covariances (either for the background or the analysis) in order to decrease the confidence in model forecasts. "Additive inflation" adds a small multiple of the identity matrix to the background covariance or the analysis covariance during each data assimilation cycle (Ott *et al.* (2002, 2004)). In my studies, a "multiplicative inflation", denoted as ρ (Anderson and Anderson (1999); Hamill *et al.* (2001)), is used to multiply the background perturbation matrix, $\mathbf{X}^b$, during each assimilation cycle. Normally, ρ is set equal to 1 meaning that there is no inflation. If a factor $\rho > 1$ is applied, then the influence of past observations on future analyses will decrease exponentially over time.

2.4 Ensemble Smoothing

Ensemble-based methods in data assimilation such as the EnKF (Evensen (1994, 2009a,b)) have been widely used for parameter estimations in the reservoir-engineering community. As an alternative to the EnKF, ensemble smoothing (ES) is another popular method that has been used to build applications for history matching reservoir models. The reader can refer to Aanonsen *et al.* (2009) for a comprehensive review for those applications. Skjervheim *et al.* (2011) have used both EnKF and ES for history matching reservoir models and showed similar results and performances from the two methods in a reservoir test case.

Ensemble smoothing solves the same formulation of the cost function as EnKF, i.e., maximum likelihood. In the context of reservoir history-matching problems, the model uncertainty is often ignored as reservoir models are usually stable functions of the rock property fields (Emerick and Reynolds (2013)). Thus, ES is often applied to solve only the parameter-estimation problem for reservoir simulation models.

Similarly, in this dissertation, ES is applied to solve the parameter-estimation problem for specific reduced-order models, i.e., the ES only updates some parameters of a reduced-order model. Consequently, in the context of ES, the input of Equation (2.14) becomes a vector of chosen model parameters instead of model state variables. The updated parameters for a model given by ES can be used to simulate the model in order to improve the model predictions.

A major difference between the ES and the EnKF is how data are assimilated into model forecasts. The ES assimilates all data including both past and future observations at once to generate a global update for selected model parameters, whereas the EnKF is a recursive algorithm that updates the system state sequentially as new data become available in real time. The data are seen as the history of a dynamical

system rather than incoming new observations in the context of ES. That is why ES is useful to solve history matching problems.

The method used in this thesis is called ensemble smoother with multiple data assimilation (ES-MDA) developed in Emerick and Reynolds (2013), which is an iterative version of the ES. The ES is proven to have identical performances as the EnKF for linear dynamical models and observation operators by Evensen (2004). However, for nonlinear dynamical models, the EnKF provides much better results than the ES (Evensen and Van Leeuwen (2000)). Thus, ES-MDA modifies the one-step ensemble smoothing to be an iterative method, so that the iterations can help the model to effectively update the prediction uncertainties. In sections below, we first start with stating the history matching problem formulated in the petroleum industry, and then present the solutions proposed by ES-MDA.

2.4.1 History Matching Problem

Generally, the history matching problem is a standard inverse problem. Given some measurements and a dynamical model of a system, we want to estimate the model parameters using the measurements. Assume that the model parameters and measurements are drawn from Gaussian distributions. A Bayesian formulation of the problem is presented here.

Suppose a perfect model is provided for a dynamical system

$$\mathbf{y} = \mathbf{G}(\mathbf{x}), \tag{2.26}$$

where $\mathbf{x}$ is an n-dimensional vector of model parameters and $\mathbf{y}$ is an m-dimensional predicted measurements. Let $\mathbf{d} \in \mathbb{R}^m$ be the real measurements with the following relationship to $\mathbf{y}$

$$\mathbf{d} = \mathbf{y} + \epsilon, \tag{2.27}$$

where ϵ is assumed to be a Gaussian error. The problem to be solved consists of estimating the most likely values of the model parameters $\mathbf{x}$ based on measurements and model forecasts. Using Bayes' theorem and a perfect forward model, the joint posterior PDF for $\mathbf{x}$ and $\mathbf{y}$ is defined as

$$\begin{aligned} f(\mathbf{x},\mathbf{y}|\mathbf{d}) &\propto f(\mathbf{x},\mathbf{y})f(\mathbf{d}|\mathbf{y}) \\ &= f(\mathbf{x})f(\mathbf{y}|\mathbf{x})f(\mathbf{d}|\mathbf{y}) \\ &= f(\mathbf{x})\delta(\mathbf{y}-\mathbf{G}(\mathbf{x}))f(\mathbf{d}|\mathbf{y}), \end{aligned} \tag{2.28}$$

where the transition density $f(\mathbf{y}|\mathbf{x})$ is the Dirac delta function under the assumption of a perfect model (no model error). In order to obtain the marginal PDF for $\mathbf{x}$, we integrate Equation (2.28) over $\mathbf{y}$, which gives the posterior PDF of the parameters

$$\begin{aligned} f(\mathbf{x}|\mathbf{d}) \propto & \int f(\mathbf{x})\delta(\mathbf{x}-\mathbf{G}(\mathbf{x}))f(\mathbf{d}|\mathbf{y})d\mathbf{y} \\ =& f(\mathbf{x})f(\mathbf{d}|\mathbf{G}(\mathbf{x})). \end{aligned} \tag{2.29}$$

Assume that both the prior $f(\mathbf{x})$ and likelihood $f(\mathbf{d}|\mathbf{G}(\mathbf{x}))$ are Gaussian. Then, the marginal PDF becomes

$$f(\mathbf{x}|\mathbf{d}) \propto \exp\left[-\frac{1}{2}\left((\mathbf{x}-\mathbf{x}^f)^T\mathbf{C}_{xx}^{-1}(\mathbf{x}-\mathbf{x}^f)+(\mathbf{G}(\mathbf{x})-\mathbf{d})^T\mathbf{C}_{dd}^{-1}(\mathbf{G}(\mathbf{x})-\mathbf{d})\right)\right], \tag{2.30}$$

where $\mathbf{x}^f$ is the prior estimate for $\mathbf{x}$, $\mathbf{C}_{xx}$ is the $n \times n$ error covariance matrix of $\mathbf{x}^f$, and $\mathbf{C}_{dd}$ is the $m \times m$ error covariance matrix of the measurements $\mathbf{d}$. Maximizing Equation (2.30) is equivalent to minimize the cost function

$$J(\mathbf{x}) = \left(\mathbf{x}-\mathbf{x}^f\right)^T\mathbf{C}_{xx}^{-1}\left(\mathbf{x}-\mathbf{x}^f\right)+(\mathbf{G}(\mathbf{x})-\mathbf{d})^T\mathbf{C}_{dd}^{-1}(\mathbf{G}(\mathbf{x})-\mathbf{d}). \tag{2.31}$$

This cost function is similar to the one defined for KF in a linear case, Equation (2.14). In the case that $\mathbf{G}$ is a linear model, the minimizer for Equation (2.31) is

given by the standard KF update equations

$$\mathbf{x}^a = \mathbf{x}^f + \mathbf{K}(\mathbf{d} - \mathbf{G}\mathbf{x}), \tag{2.32}$$

$$\mathbf{C}_{xx}^a = (\mathbf{I} - \mathbf{K}\mathbf{G})\mathbf{C}_{xx}, \tag{2.33}$$

$$\mathbf{K} = \mathbf{C}_{xx}\mathbf{G}(\mathbf{G}\mathbf{C}_{xx}\mathbf{G}^T + \mathbf{C}_{dd})^{-1}, \tag{2.34}$$

which produce the analysis update (superscript a stands for analysis).

Now continue with the linear case but considering an ensemble representation of the error covariances

$$\mathbf{C}_{xx}^e = \mathbf{A}\mathbf{A}^T/(n_e - 1), \tag{2.35}$$

where n_e is the number of ensemble members and $\mathbf{A}$ is analogous to the background perturbation matrix $\mathbf{X}^b$ as in EnKF: each column of A is given by the difference between each prior ensemble member and the ensemble mean. Then, Equations (2.32) and (2.34) can be rewritten as

$$\mathbf{x}_j^a = \mathbf{x}_j^f + \mathbf{K}^e(\mathbf{d}_j - \mathbf{G}\mathbf{x}_j), \tag{2.36}$$

$$\mathbf{K}^e = \mathbf{C}_{xx}^e\mathbf{G}(\mathbf{G}\mathbf{C}_{xx}^e\mathbf{G}^T + \mathbf{C}_{dd})^{-1}, \tag{2.37}$$

where $\mathbf{x}_j$ and $\mathbf{d}_j$, are a pair of ensemble realizations, and $\mathbf{d}_j = \mathbf{d}_j + \epsilon_j$ denotes the perturbed observations (Burgers *et al.* (1998)). The noise ϵ_j is sampled out of a Gaussian distribution with mean $\mathbf{0}$ and covariance $\mathbf{C}_{dd}$. Evensen has shown that with an infinite size of the ensemble, the update in Equation (2.36) implies Equation (2.33) (Evensen (2009a)). It is also easy to show that the solutions Equations (2.36) and (2.37) can be obtained by solving the alternative cost function defined as

$$J(\mathbf{x}_j) = \left(\mathbf{x}_j - \mathbf{x}_j^f\right)^T \mathbf{C}_{xx}^{-1} \left(\mathbf{x}_j - \mathbf{x}_j^f\right) + (\mathbf{G}\mathbf{x}_j - \mathbf{d}_j)^T \mathbf{C}_{dd}^{-1} (\mathbf{G}\mathbf{x}_j - \mathbf{d}_j). \tag{2.38}$$

In the nonlinear case, the cost function in (2.38) becomes

$$J(\mathbf{x}_j) = \left(\mathbf{x}_j - \mathbf{x}_j^f\right)^T \mathbf{C}_{xx}^{-1} \left(\mathbf{x}_j - \mathbf{x}_j^f\right) + (\mathbf{G}(\mathbf{x}_j) - \mathbf{d}_j)^T \mathbf{C}_{dd}^{-1} (\mathbf{G}(\mathbf{x}_j) - \mathbf{d}_j), \tag{2.39}$$

where the sampled posterior will be non-Gaussian due to the nonlinear model $\mathbf{G}(\mathbf{x})$. Consequently, the analysis update equations become

$$\mathbf{x}_j^a = \mathbf{x}_j^f + \mathbf{K}^e \left(\mathbf{d}_j - \mathbf{G}\left(\mathbf{x}_j^f\right)\right), \tag{2.40}$$

$$\mathbf{K}^e = \mathbf{C}_{xx}^e \mathbf{G}'(\mathbf{x}^f)(\mathbf{G}'(\mathbf{x}^f)\mathbf{C}_{xx}^e \mathbf{G}'(\mathbf{x}^f)^T + \mathbf{C}_{dd})^{-1}, \tag{2.41}$$

where the tangent-linear operator $\mathbf{G}'$ is approximated at the mean of the prior ensemble. Equations (2.40) and (2.41) are also known as the standard ensemble smoothing update equations.

2.4.2 Ensemble Smoother with Multiple Data Assimilation

The ES-MDA solves the Bayesian formulation of the history matching problem using a tempering procedure of the likelihood function in Equation (2.29) (Neal (1996); Stordal and Elsheikh (2015)). In ES-MDA, the likelihood function for measurements is rewritten as

$$f(\mathbf{d}|\mathbf{y}) = f(\mathbf{d}|\mathbf{y})^{\sum_{i=1}^{N_{\text{mda}}} \frac{1}{\alpha_i}} = \prod_{i=1}^{N_{\text{mda}}} f(\mathbf{d}|\mathbf{y})^{\frac{1}{\alpha_i}}, \tag{2.42}$$

where

$$\sum_{i=1}^{N_{\text{mda}}} \frac{1}{\alpha_i} = 1. \tag{2.43}$$

Under the same Gaussian assumption, the likelihood becomes

$$f(\mathbf{d}|\mathbf{y}) \propto \exp\left(-\frac{1}{2}(\mathbf{y}-\mathbf{d})\mathbf{C}_{dd}^{-1}(\mathbf{y}-\mathbf{d})\right) \tag{2.44}$$

$$= \prod_{i=1}^{N_{\text{mda}}} \exp\left(-\frac{1}{2\alpha_i}(\mathbf{y}-\mathbf{d})\mathbf{C}_{dd}^{-1}(\mathbf{y}-\mathbf{d})\right). \tag{2.45}$$

Plug in the likelihood in Equation (2.29), we get

$$f(\mathbf{x}|\mathbf{d}) \propto f(\mathbf{x}) \prod_{i=1}^{N_{\text{mda}}} f(\mathbf{d}|\mathbf{G}(\mathbf{x}_{i-1}))^{\frac{1}{\alpha_i}}. \tag{2.46}$$

This equation can also be rewritten in a recursive manner, starting with the prior $\mathbf{x} = \mathbf{x}_0$ leading to the posterior $\mathbf{x} = \mathbf{x}_{N_{\text{mda}}}$:

$$\begin{aligned} f(\mathbf{x}_1|d) \propto & f(\mathbf{x}_0) f(\mathbf{d}|\mathbf{G}(\mathbf{x_0}))^{\frac{\mathbf{1}}{\alpha_\mathbf{1}}}, \\ f(\mathbf{x}_2|d) \propto & f(\mathbf{x}_1|\mathbf{d}) f(\mathbf{d}|\mathbf{G}(\mathbf{x_1}))^{\frac{\mathbf{1}}{\alpha_\mathbf{2}}}, \\ & \vdots \\ f(\mathbf{x}_{N_{\text{mda}}}|d) \propto & f(\mathbf{x}_{N_{\text{mda}-1}}|\mathbf{d}) f(\mathbf{d}|\mathbf{G}(\mathbf{x}_{N_{\text{mda}-1}})^{\frac{1}{\alpha_{N_{\text{mda}}}}}. \end{aligned} \tag{2.47}$$

The KF update equations are applied to minimize a cost function for each recursive step. Thus, the ES-MDA solves a predefined sequence of cost functions that are similar to the cost function defined in Equation (2.31), which are defined as

$$\begin{aligned} J(\mathbf{x}_{j,i+1}) = & (\mathbf{x}_{j,i+1} - \mathbf{x}_{j,i}) \left(\mathbf{C}_{xx}^{e,i}\right)^{-1} (\mathbf{x}_{j,i+1} - \mathbf{x}_{j,i}) \\ & + (\mathbf{G}(\mathbf{x}_{j,i+1}) - \mathbf{d} - \sqrt{\alpha_i}\epsilon_j) \\ & \times (\alpha_i \mathbf{C}_{dd}^{e})^{-1} (\mathbf{G}(\mathbf{x}_{j,i+1}) - \mathbf{d} - \sqrt{\alpha_i}\epsilon_j), \end{aligned} \tag{2.48}$$

where $j = 1, \ldots, n_e, i = 1, \ldots, N_{\text{mda}}$, and the initial $(\mathbf{C}_{xx}^{e})_{i=1} = \mathbf{C}_{xx}^{e}$ and $\mathbf{x}_{j,i=1} = \mathbf{x}_j^f$. In each recursive step, ES-MDA inflates the measurement errors by a factor $\sqrt{\alpha_i}$ to reduce the impact of the measurements.

The standard ES Equations (2.40-2.41) are used to solve the sequence of cost functions stated above. With the inflated measurement errors, the analysis update at each recursive step for individual ensemble member becomes

$$\begin{aligned} \mathbf{x}_{j,i+1} = & \mathbf{x}_{j,i} + \mathbf{G}'(\mathbf{x}_{j,i}) \mathbf{C}_{xx}^{e,i} \left(\mathbf{G}'(\mathbf{x}_{j,i}) \mathbf{C}_{xx}^{e,i} \mathbf{G}'(\mathbf{x}_{j,i}) + \alpha_i \mathbf{C}_{dd}^{e}\right)^{-1} \\ & \times (\mathbf{d} + \sqrt{\alpha_i}\epsilon_j - \mathbf{G}(\mathbf{x}_{j,i})). \end{aligned} \tag{2.49}$$

After getting the updated parameters $\mathbf{x}_{j,i+1}$, the model is rerun with updated parameters to get a posterior ensemble of model predictions (predicted measurements given by model)

$$\mathbf{y}_{j,i+1} = \mathbf{G}(\mathbf{x}_{j,i+1}), \tag{2.50}$$

which will be used to approximate the tangent-linear operator $\mathbf{G}'$ for the next iteration. The final output of parameters is after N_{mda} steps where $\mathbf{x}_j^a = \mathbf{x}_{j,N_{\text{mda}}}$. The model is rerun with the final updated parameters to generate the final history-matched ensemble of model predictions. This iterative scheme of the ensemble smoothing is expected to have better performance than one long update step in standard ensemble smoother, because it uses many short linear steps to help reduce the errors.

Chapter 3

A REDUCED-ORDER MODEL OF PROSTATE CANCER UNDER ANDROGEN SUPPRESSION THERAPY

3.1 Androgen Suppression Therapy

Prostate cancer is the second leading cause of cancer death in American men according to the American Cancer Society. On average, one in every eight American men will be diagnosed with prostate cancer in his life time (ACS (2021)). Much progress has been made in treatment for prostate cancer over the years to improve patients' symptoms and quality of life.

In 1941, Huggins and Hodes (Ch and Hodges (1941)) discovered that castration induces the regression of prostate tumors which led to the conclusion that the growth of prostate tumors is highly dependent on male hormones, called the androgen. Their study suggested the first time that some cancers could be treated by chemical means. Huggins shared the 1966 Nobel Prize for Physiology or Medicine because of this discovery. Currently, hormonal therapy, in particular the androgen suppression therapy, is a regular treatment option for prostate cancers especially for metastasized cases (Kumar *et al.* (2006)).

Generally in androgen suppression therapy, drugs are administrated continuously to a patient, which is known as the continuous androgen suppression therapy (CAS) (Feldman and Feldman (2001)). However, like any kind of drugs, the tumor develops drug resistance eventually. In addition, CAS also causes long-term side effects such as muscle loss, bone demineralization, and dementia. Consequently, intermittent

androgen suppression therapy (IAS) has been tested as a way to delay the onset of hormonal resistance and reduce the side effects for a patient (Spry *et al.* (2006)).

IAS will pause the treatment if a patient's blood serum level of prostate-specific antigen (PSA), a biomarker for prostate cancer, falls below a certain threshold as determined by his doctor. Likewise, the patient receives treatment if his PSA level arises above an upper predetermined level. Clinical measurements of PSA and serum androgen are usually taken monthly to assess a patient's treatment results. The on-treatment and off-treatment cycles are repeated until the tumor develops resistance. One round of IAS therapy is considered as one consecutive on-and-off treatment cycle.

3.2 Modeling for IAS Treatment Response

The most important question in IAS therapy is whether another round of IAS will be effective to treat the cancer. Based on a patient's past treatment results, how can one extract useful information to make a sensible decision for the short future? If the doctor and patient know beforehand that another round of IAS would not work, then they could look for a different treatment option to make the most out of time and resources. To answer these fundamental questions, a predictive model that can produce accurate short-term forecasts of treatment response is much needed.

3.2.1 Brief History of Model Development for Prostate Cancer

Over the past 20 years, various mathematical models have been developed to aid with our understanding of prostate tumor dynamics with or without treatment. The article by Phan *et al.* (2020) gives a comprehensive overview of available mathematical models for prostate cancer under different types of therapies. Most of these models are simplified low-dimensional models that can be used to test different hypotheses of the tumor dynamics.

One early model by Yorke *et al.* (1993) is a kinetic model that treats the tumor as one uniform system and describes how it interacts with local treatments such as radiation therapy. Later models adapted the theory of population dynamics by treating the tumor as a combination of different cancer cell subpopulations. For example, Ideta *et al.* (2008) suggested the idea of an androgen dependent (treatment sensitive) subpopulation and an androgen independent (treatment insensitive) subpopulation to represent the tumor. These two subpopulations were modeled individually via ordinary differential equations with the assumption that androgen dependent cells can transform into androgen independent cells. Ideta *et al.* used their model to study and compare tumor dynamics under the two therapies: CAS and IAS. Early development of mathematical models for prostate cancer mostly focused on understanding possible mechanism of prostate tumor growth by considering various assumptions. However, these older models do not include clinical data in its modeling process which hinders validation of the model.

Hirata *et al.* (2010) first developed a data-driven model to generate simulations that recover the real clinical data of PSA levels. They built a piecewise linear model for the IAS therapy that includes three cancer cell subpopulations: treatment-sensitive, treatment-insensitive, and irreversibly treatment-insensitive cells. They assumed that all the interactions among different cell subpopulations happen in a linear manner. The model takes different forms during on and off treatments. When a patient is on treatment, their models takes the form:

$$\frac{d}{dt}\begin{pmatrix} x_1(t) \\ x_2(t) \\ x_3(t) \end{pmatrix} = \begin{pmatrix} w^1_{1,1} & 0 & 0 \\ w^1_{2,1} & w^1_{2,2} & 0 \\ w^1_{3,1} & w^1_{3,2} & w^1_{3,3} \end{pmatrix} \begin{pmatrix} x_1(t) \\ x_2(t) \\ x_3(t) \end{pmatrix}. \tag{3.1}$$

When a patient is off treatment, the model takes the form:

$$\frac{d}{dt}\begin{pmatrix} x_1(t) \\ x_2(t) \\ x_3(t) \end{pmatrix} = \begin{pmatrix} w^0_{1,1} & w^0_{1,2} & 0 \\ 0 & w^0_{2,2} & 0 \\ 0 & 0 & w^0_{3,3} \end{pmatrix} \begin{pmatrix} x_1(t) \\ x_2(t) \\ x_3(t) \end{pmatrix}. \tag{3.2}$$

Treatment-sensitive, treatment-insensitive, and irreversibly treatment-insensitive cell populations are denoted by x_1, x_2 and x_3, respectively. The weight parameters $w_{ij}, i, j \in \{1, 2, 3\}$, are transformation rates from x_i to x_j. Notice that the weight parameters of on and off treatments are different. This model also assumes that the PSA level (denoted as P) is produced proportionally to the sum of the subpopulations:

$$P(t) = \alpha(x_1(t) + x_2(t) + x_3(t)). \tag{3.3}$$

The linear model can be chosen to reproduce individual patient's PSA level during IAS therapy. However, the Hirata model does not explain well the biological mechanism of tumor dynamics under the IAS therapy.

As an improvement from Hirata's approach, Portz *et al.* (2012) created a more biologically mechanistic model that also includes the clinical measurements in its modeling procedure. Their model assumed that androgen is the main limiting nutrient to feed the tumor and considered the two cell subpopulations of androgen dependent (AD) and androgen independent (AI) cells. The nutrient-limiting theory was first established by Droop (1968) in the context of marine ecology which introduced the terminology "cell quota" to refer to the limiting nutrient. In the context of prostate cancer, cell quota represents the minimum androgen level required for each cell subpopulation to survive and grow. The model allows for the possibility that the transformation between the AD and AI subpopulations is reversible. The model

takes the final form of five ordinary differential equations:

$$\frac{dx_1}{dt} = \underbrace{\mu_m\left(1-\frac{q_1}{Q_1}\right)x_1}_{\text{growth}} - \underbrace{d_1x_1}_{\text{death}} - \underbrace{c_1\lambda_1(Q_1)x_1 + c_2\lambda_2(Q_2)x_2}_{\text{mutation}}, \tag{3.4}$$

$$\frac{dx_2}{dt} = \underbrace{\mu_m\left(1-\frac{q_2}{Q_2}\right)x_2}_{\text{growth}} - \underbrace{d_2x_2}_{\text{death}} - \underbrace{c_2\lambda_2(Q_2)x_2 + c_1\lambda_1(Q_1)x_1}_{\text{mutation}}, \tag{3.5}$$

$$\frac{dQ_1}{dt} = \underbrace{v_m\left(\frac{q_m-Q_1}{q_m-q_1}\right)\left(\frac{A(t)}{A(t)+v_h}\right)}_{\text{androgen influx to } x_1 \text{ cells}} - \underbrace{\mu(Q_1-q_1)}_{x_1 \text{ androgen uptake}} - \underbrace{bQ_1}_{\text{degradation}}, \tag{3.6}$$

$$\frac{dQ_2}{dt} = \underbrace{v_m\left(\frac{q_m-Q_2}{q_m-q_2}\right)\left(\frac{A(t)}{A(t)+v_h}\right)}_{\text{androgen influx to } x_2 \text{ cells}} - \underbrace{\mu(Q_2-q_2)}_{x_2 \text{ androgen uptake}} - \underbrace{bQ_2}_{\text{degradation}}, \tag{3.7}$$

$$\frac{dP}{dt} = \underbrace{\sigma(x_1+x_2)}_{\text{baseline PSA production}} + \underbrace{\frac{\sigma_1x_1Q_1^m}{Q_1^m+\rho_1^m} + \frac{\sigma_2x_2Q_2^m}{Q_2^m+\rho_2^m}}_{\text{tumor PSA production}} - \underbrace{\delta P}_{\text{degradation}}. \tag{3.8}$$

Here the variables x_1 and x_2 denotes the AD and AI subpopulations, respectively. The variables Q_1 and Q_2 denotes the respective intracellular androgen level (androgen available inside the cell) for AD and AI cells. PSA level is denoted by the variable P. The cell quota concept is coded in the parameters q_1 and q_2 to represent the minimum androgen level required for each cell subpopulation to grow. The basic idea of the model is that when $Q < q$, the subpopulation is expected to decrease; when $Q > q$ the subpopulation will grow. Another important feature of this model is that $A(t)$, the blood serum androgen level, is a time-dependent parameter obtained by interpolating the real clinical data of serum androgen. Usually every patient will be taken measurements of both PSA and blood serum androgen throughout the treatment journey.

The "Portz model" describes the underlying biological mechanism meanwhile reproduces the clinical data of PSA for model validation. This model has motivated more later studies by Baez and Kuang (2016) and Phan *et al.* (2019) where both

studies used the structure of the Portz model but modified different assumptions of the original model. In this thesis, the model I focus on is developed by Phan *et al.* (2019), which is referred as the Model T hereafter.

Model T was built upon a simplified version of the Portz model developed in Baez and Kuang (2016). Baez and Kuang assumed that the mutation between the AD and AI subpopulations is irreversible: only AD cells can mutate into AI cells. Model T adapted this assumption as well. Furthermore, Model T included the clinical data of serum androgen directly in its model state which is represented by the variable A. Model T is described as:

$$\frac{dx_1}{dt} = \underbrace{\mu_1\left(1-\frac{q_1}{Q}\right)x_1}_{\text{growth}} - \underbrace{\left(D_1(Q)+\delta_1 x_1\right)x_1}_{\text{death}} - \underbrace{\lambda(Q)x_1}_{\text{mutation}}, \tag{3.9}$$

$$\frac{dx_2}{dt} = \underbrace{\mu_2\left(1-\frac{q_2}{Q}\right)x_2}_{\text{growth}} - \underbrace{\left(D_2(Q)+\delta_2 x_2\right)x_2}_{\text{death}} + \underbrace{\lambda(Q)x_1}_{\text{mutation}}, \tag{3.10}$$

$$\frac{dQ}{dt} = \underbrace{m(A-Q)}_{\text{androgen diffusion A}\to\text{Q}} - \underbrace{\frac{\mu_1(Q-q_1)x_1+\mu_2(Q-q_2)x_2}{x_1+x_2}}_{\text{androgen uptake}}, \tag{3.11}$$

$$\frac{dA}{dt} = \underbrace{\gamma_2+\gamma_1(A_0-A)}_{\text{production}} \quad \underbrace{-A_0\gamma_1 u(t)}_{\text{suppression of production}}, \tag{3.12}$$

$$\frac{dP}{dt} = \underbrace{bQ}_{\text{baseline PSA production}} + \underbrace{\sigma(Qx_1+Qx_2)}_{\text{tumor PSA production}} - \underbrace{\epsilon P}_{\text{degradation}}. \tag{3.13}$$

Model T was specifically created for the IAS therapy. The on-treatment and off-treatment cycles are controlled by the parameter $u(t)$ in the equation for serum androgen, A. When the patient is on treatment, $u(t)$ equals to 1 and equals to 0 otherwise. The advantage of Model T in comparison to previous models is that it utilizes all available information from clinical measurements which could enhance the accuracy of model predictions. In practice, PSA level of a patient is used to assess

the efficacy of the IAS therapy. Hence, I also use the predicted PSA level from the model to compare with the real clinical data so as to validate the model later.

3.2.2 Prediction Uncertainty Contributed by Parameter Identifiability

The British statistician George Box has a well-known saying about modeling (Box (1976)): "All models are wrong, but some are useful." Although many mathematical models were developed over the past 20 years to study IAS treatment, the question of how useful these models are in clinical applications is unexplored. In the context of intermittent androgen suppression therapy, patients and doctors rely on an accurate model forecast on patient's short-term treatment response in order to decide the best treatment plan for a patient. This practice is an example of precision (personalized) medicine. Thus, assessment and validation of a model's prediction skills are vital to integrate the theoretical approach with the real-world application.

Parameters of a mathematical model play an important role in the model's performance. In order to achieve the goal of personalized medicine for prostate cancer patients, patient-specific model parameters must be estimated. Phan *et al.* (2019) has a detailed discussion on how parameters of the Model T are estimated – either from previous literature reviews or directly estimated from the clinical data. As Table 3.1 shows the original parameter ranges for Model T, the variability of each parameter is large. Individual parameter could be different by factor of 10 to 1000.

Now a reasonable question based on Table 3.1 could be: how can we have confidence in the parameter estimates while the range is so wide? A common challenge encountered by most of the mathematical models for prostate cancers is that model parameters may not be identifiable for a given data set, i.e., we cannot obtain unique parameter values for a specific patient given only time series of PSA levels and possibly serurm androgen levels. This problem is known as the parameter identifiability.

Param	Description	Range	Unit
μ	max proliferation rate	$0.001 - 0.09$	$[day]^{-1}$
μ_1	max proliferation rate (AD cells)	$0.001 - 0.09$	$[day]^{-1}$
μ_2	max proliferation rate (AI cells)	$0.001 - 0.09$	$[day]^{-1}$
q_1	min AD cell quota	$0.41 - 1.73^{**}$	$[nmol][day]^{-1}$
q_2	min AI cell quota	$0.01 - 0.41^{**}$	$[nmol][day]^{-1}$
b	baseline PSA production rate	$0.0001 - 0.1$	$[\mu g][nmol]^{-1}[day]^{-1}$
σ	tumor PSA production rate	$0.001 - 1$	$[\mu g][nmol]^{-1}[L]^{-1}[day]^{-1}$
ϵ	PSA clearance rate	$0.0001 - 0.1$	$[day]^{-1}$
d_1	max AD cell death rate	$0.001 - 0.09$	$[day]^{-1}$
d_2	max AI cell death rate	$0.01 - 0.001$	$[day]^{-1}$
δ_1	density death rate	$1 - 90^{*}$	$[L]^{-1}[day]^{-1}$
δ_2	density death rate	$1 - 90^{*}$	$[L]^{-1}[day]^{-1}$
R_1	AD death rate half-saturation	$0 - 3$	$[nmol][L]^{-1}$
R_2	AI death rate half-saturation	$1 - 6$	$[nmol][L]^{-1}$
c	maximum mutation rate	$0.00001 - 0.0001^{*}$	$[day]^{-1}$
K	mutation rate half-saturation level	$0.8 - 1.7^{*}$	$[nmol][day]^{-1}$
γ_1	primary androgen production rate	$0.008 - 0.8$	$[day]^{-1}$
γ_2	secondary androgen production rate	$0.001 - 0.1^{*}$	$[day]^{-1}$
m	diffusion rate from A to Q	$0.01 - 0.9$	$[day]^{-1}$
A_0	maximum serum androgen level	$27 - 35^{**}$	$[nmol][day]^{-1}$
$x_1(0)$	Initial population of AD cells	$0.009 - 0.02$	$[L]$
$x_2(0)$	Initial population of AI cells	$0.0001 - 0.001$	$[L]$

Table 3.1: Parameter ranges for Model T. Table 2 from Phan *et al.* (2019), used with permission. Parameters with an asterisk are fixed for the model; parameters with double asterisks are estimated from the first 1.5 cycles of clinical data using a built-in MATLAB function *fmincon*.

Wu *et al.* (2019) has proven analytically using the Fisher information matrix (Eisenberg and Hayashi (2014); Miao *et al.* (2011)) that neither the "Hirata model" nor the "Portz model" is identifiable.

Models with unidentifiable parameter(s) can still fit the clinical data well. However, the uncertainty in future forecasts produced by such unidentifiable models can be large. Figure 3.1 demonstrates the prediction uncertainty in both the Hirata model (Model H) and the Portz model (Model P) for a particular patient time series of PSA. The patient data is provided in Bruchovsky *et al.* (2006). Wu *et al.* (2019) used five different sets of parameters for both Model H and Model P to first fit the clinical data of the same patient (about first 900 days of treatment) then to predict the rest of the treatment response. The "optimal" sets of parameters are obtained by a MATLAB built-in function called *fmincon*, which is a mean-squared-error parameter estimation method. For Model H, the five sets of parameters are obtained by varying the parameter w_{11}^0 over a $\pm 10\%$ range of the optimal set. For Model P, the five sets of parameters are obtained by varying μ_m over a $\pm 10\%$ range of the optimal set.

As Figure 3.1 shows that different sets of parameters can give comparable good fitting results over the first 1.5 treatment cycles of the same patient. However, using the same sets of parameters to predict another treatment cycle, most of the predictions diverge quickly from the real clinical data except for one parameter set in Model P. The predictions given by five parameter sets for each model often overestimate the real PSA level of the patient and also show a spread among themselves. This finding by Wu *et al.* (2019) suggests that unidentifiable models may not be able to produce reliable short-term forecasts for clinical applications. The concern of prediction uncertainty in unidentifiable models motivates us to look for a more identifiable model and also quantify the model's forecast uncertainty via data assimilation. The data assimilation scheme chosen for this application is the ensemble Kalman filter (EnKF).

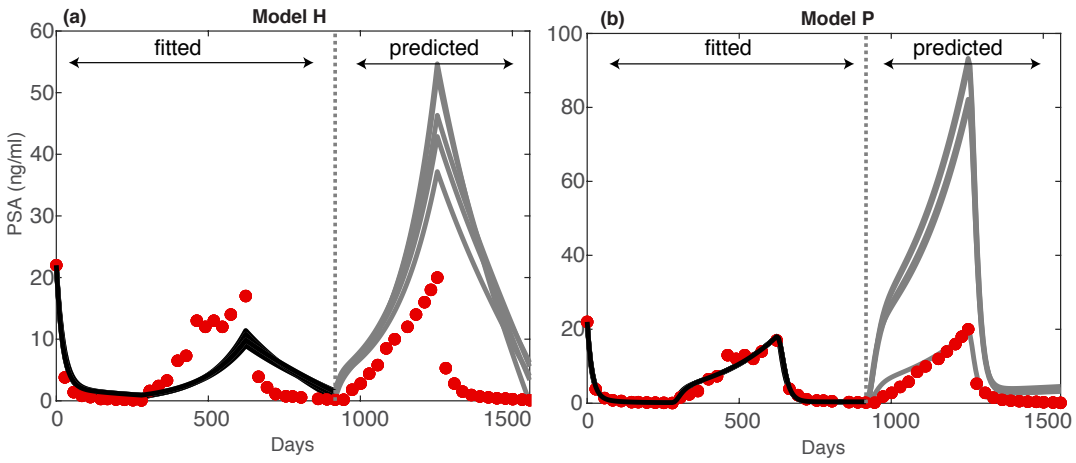

Figure 3.1: Fitting and prediction results obtained from Model H and Model P. Figure 1 in Wu *et al.* (2019), used with permission. The left of the dotted vertical line is the fitting results of different parameter sets; the right of the dotted line is the prediction results. Red dots are clinical data of the same patient. For both models, the "optimal" fitting parameter set are generated by MATLAB built-in function *fmincon*. **(a)** Model H results. **(b)** Model P results. Data are provided by Bruchovsky *et al.* (2006).

3.3 Data Assimilation with an Identifiable Model

As discussed in the previous section that unidentifiable models can suffer from large uncertainty in short-term predictions, so we want to look for an identifiable model to reduce the uncertainty. The model we are interested in studying is Model T.

Model T has 21 parameters in total together with a 5-dimensional state vector. Phan *et al.* (2019) carried a sensitivity analysis on all parameters of Model T. According to their study, these five parameters: c, K, δ_1, δ_2, and γ_2 do not influence significantly the results of model simulations. Thus, these five parameters are fixed

at $c = 0.00015, K = 1, \delta_1 = 5, \delta_2 = 5, \gamma_2 = 0.005$ throughout the study. Furthermore, Wu *et al.* (2019) also simplified the model by setting $\mu_1 = \mu_2 = \mu_m$. Then there are 13 parameters left which is referred as Model T-13. Wu *et al.* (2019) analytically showed that Model T-13 is still unidentifiable using the Fisher information matrix. This leads to a further reduction of the parameter space by leaving only 5 most sensitive parameters unfixed, which gives a new version of the model called Model T-5. These 5 free parameters are: $\mu_m, q_2, d_1, \gamma_1$, and A_0. According to the analysis in Wu *et al.* (2019), Model T-5 is identifiable, which is used to design the data assimilation scheme.

3.3.1 Data and Parameter Values

The clinical data is provided by Vancouver Prostate Center, which admitted patients who experienced a rising serum PSA level after they received radiotherapy and had no evidence of metastasis (Bruchovsky *et al.* (2006)). These patients have not had hormonal suppression therapy with the exception of less than 3 months of neoadjuvant androgen-suppression. Their PSA levels prior to the therapy are usually high (greater than $6\mu g/L$). Moreover, they must have experienced PSA relapses after radiotherapy with no evidence of distant metastasis such as bone metastasis.

In this study, two subsets of patients are selected from the clinical study in Bruchovsky *et al.* (2006). The first subset contains 28 patients with complete data for at least one cycle of treatment. This set is used to estimate the statistics (mean and variance of 28 patients) of each parameter to initialize the EnKF. The second subset contains 26 patients (selected outside of the previous 28 patients) with complete data for 2.5 cycles of treatment. The latter data set is used for assessment of the model's prediction skill (predictability).

The first data set is used to generate the sample statistics of parameters in Model T-13 with a built-in MATLAB function called *fmincon*. This function minimizes the mean squared error of predicted PSA given by model and corresponding real observations to search for the optimal combination of parameters, i.e., the parameter set is generated all at once as a final output of the function. Table 3.2 shows the results of estimated mean and variance out of the 28 patients for each parameter in Model T-13. The mean of each parameter is used as either the value of fixed parameters in Model T-5 or initial condition for developed EnKF algorithm.

Parameter	μ_m	q_1	q_2	b	d_1	R_1	
mean	0.0710	0.6130	0.1971	0.0379	0.0687	1.2499	
var	0.0006	0.0111	0.0091	0.0008	0.0005	0.4059	
Parameter	γ_1	σ	ϵ	A_0	d_2	R_2	m
mean	0.3742	0.8667	0.0565	11.63	0.0633	2.7351	0.7188
var	0.0928	0.0680	0.0006	23.69	0.0006	1.2527	0.0604

Table 3.2: Parameter estimations from the 28 patients after running *fmincon*. Table 2 in Wu *et al.* (2019), used with permission.

3.3.2 State-parameter Estimation of Model T-5 with Ensemble Kalman Filter

Data assimilation is useful to quantify the errors in model forecasts and parameter estimations for Model T-5. The ultimate goal of using data assimilation is to generate corrected predictions of the treatment response by combining the mathematical model with real clinical data (PSA and serum androgen).

Data assimilation usually is used to update the state of a dynamical system directly, but the 5 unfixed parameters of Model T-5 also require correct estimations to uncover the underlying mechanism of tumor dynamics for an individual patient. State-parameter estimation within the data assimilation framework can be used to

update the parameter values of the model directly. Using the computational model and data to estimate parameters is essentially solving an inverse problem: the cause of the dynamics is inferred from the real observations.

In this thesis, the ensemble Kalman filter (EnKF) is chosen as the data assimilation framework for Model T-5. EnKF is one popular sequential data assimilation method originally proposed by Evensen (1994). It has gained much popularity ever since because of its simple conceptual formulation and efficient implementation. EnKF is a derivative of the Kalman filter (Kalman (1960)) which originally is designed for linear dynamics and assumes Gaussian distributions for system states. As an advancement from the Kalman filter, EnKF is created specifically for nonlinear dynamics and uses an ensemble of states to account for the stochastic nature of nonlinear dynamics. It also assumes that the system states are Gaussian distributed. Evensen (1994, 2003, 2009a) are good overviews of formulation and implementation for EnKF.

Moreover, in order to estimate the chosen parameters of Model T-5 in real-time, an augmented state vector is required for development of the data assimilation algorithm. The augmented state vector will include both the state variables (5-dimensional state vector) and chosen parameters of Model T-5. Whenever there is new data available from a patient's time series, the data assimilation algorithm will assimilate that data to the background forecast provided by Model T-5 and then generate the new analysis cycle (updated ensemble forecast). This analysis cycle will be used as the updated initial conditions for the next background forecast and subsequently used to calculate the next analysis cycle and so on. Throughout the course of the treatment, ensemble realizations of parameters and states are expected the converge to the "true" trajectory that recovers the real observations. The mean of the ensemble is used as the model prediction of the system.

Lastly, in order to assess the predictability of the model, each patient's data are divided into two subsets: the first 1.5 cycles of treatment as the train set, and one more subsequent treatment cycle as the test set. First, the train set is assimilated into the mathematical model via the EnKF framework, which provides updated parameters for the model. Then the last estimation (analysis cycle) of parameters is used to predict another treatment cycle so that the free model run can be used to assess prediction uncertainty (spread of the ensemble) in comparison to the test set.

Chapter 4

DATA ASSIMILATION WITH AN IDENTIFIABLE MODEL OF PROSTATE CANCER TREATMENT

4.1 Introduction

Over the past twenty years, many mathematical models have been developed to study various aspects of prostate cancer in clinical settings. Chapter 3 introduced some of these models and the challenge of parameter identifiability for these reduced-order models. It was shown in Figure 3.1 that though a model can fit past observations well, its prediction of future may not be reliable. Unidentifiable models can suffer from large uncertainty in short-term predictions.

Evaluation of a model's prediction skills is crucial for developing a useful clinical application. The most important question to be answered for intermittent androgen suppression therapy (IAS) is whether another round of IAS therapy will be effective to treat the cancer. Though numerous mathematical models have been developed over the decades to study the mechanism of prostate tumors, assessment of these models' predictive ability is not available. The goal of my study is to evaluate an identifiable reduced-order model for the IAS therapy and provide a useful clinical application that can be used to predict the short-term treatment response for an individual patient.

As stated in Chapter 3, a version of the two-cell-population model developed by Phan *et al.* (2019), called Model T-5, will be assessed using data assimilation. Model T-5 is proven to be an identifiable model for the IAS therapy in Wu *et al.* (2019). This model has 5 model variables and 5 free parameters (all other model parameters are fixed). The 5 free parameters are the most sensitive parameters according to

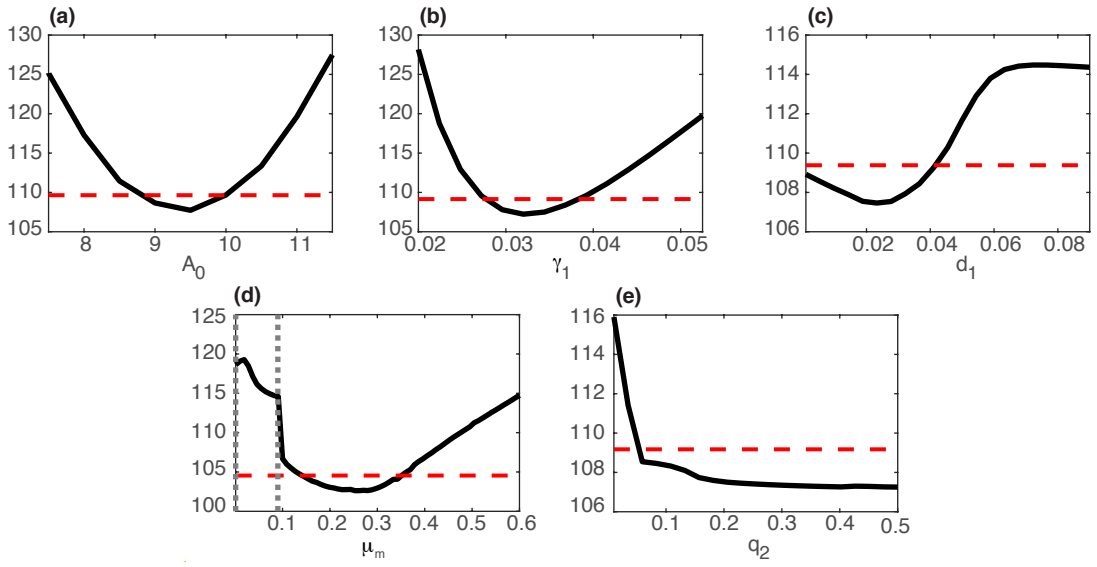

Figure 4.1: The negative log likelihood (vertical axes) of all adjustable parameters in Model T-5 in Wu *et al.* (2019). Used with permission. Intervals where the black curves lie below the red dotted line are the 95% confidence intervals. The parameter q_2 (bottom right) confidence interval lies outside of the biologically realistic ranges indicated in Table 3.1.

the sensitivity analysis in Phan *et al.* (2019). Wu *et al.* (2019) also used analytical methods such as coefficients of variation (Eisenberg and Hayashi (2014)) and profile likelihood (Eisenberg and Jain (2017); Raue *et al.* (2009)) to study the identifiability of these 5 parameters. Specifically, both methods confirm that 4 of the 5 adjustable parameters in Model T-5 may be practically identifiable. The only parameter may subject to large uncertainty is the cell quota for treatment-insensitive cell population, q_2. Shown as in Figure 4.1, the 95% confidence interval of q_2 lies beyond the biological constraint for q_2 stated in Table 3.1, which suggests that this parameter may be practically unidentifiable.

A data assimilation framework called the ensemble Kalman filter (EnKF) is used to provide state-parameter estimations for Model T-5. In particular, 3 of the 5 adjustable parameters are chosen to be estimated by the EnKF, which are A_0, γ_1 and q_2. Time series of 26 patients provided by the Vancouver Prostate Center database are used to assess the model's predictive skills. Notice that this subset of 26 patients is independent from the subset of patients used to estimate model parameters shown as in Table 3.2. Individual patient's time series are also split into two subsets to be used for different purposes: the first on-off-on treatment intervals are assimilated into the EnKF framework to provide correct parameter estimations; the subsequent off-on treatment intervals are used to compare with free model run using the parameters obtained from the EnKF. The EnKF framework is tested for all 26 patients and produces reliable predictions for most of the patients. However, there are some anomalies which show significant model error (bias). Both ideal predictions and anomalies will be included and discussed in this chapter.

4.2 Uncertainty Quantification for Model T-5

4.2.1 The Ensemble Kalman Filter

The ensemble Kalman filter (EnKF) is used here to provide state-parameter estimation for Model T-5. This type of ensemble-based data assimilation method is now state of art in a majority of operational prediction systems in the geosciences (Carrassi *et al.* (2018)) including weather prediction (Houtekamer and Zhang (2016)), and petroleum applications (Aanonsen *et al.* (2009)). The mathematical formulation of the filter is stated in Chapter 2, so the mathematical details are omitted here but the implementation of the EnKF for Model T-5 will be presented.

The EnKF is a recursive algorithm that alternates between a forecast step and an analysis (correction) step. The algorithm repeats itself at each time point when new observations become available for the system. Suppose at time t_n there is an ensemble of initial conditions, which is assumed to be a sample drawn from a Gaussian distribution about a mean state that we are interested in estimating. A background ensemble is obtained by integrating the model (Model T-5) from time t_n to t_{n+1} for each ensemble member. At time t_{n+1} new observations of the system become available, the EnKF seeks a linear combination of the background forecasts that best fits the data in a weighted least-squares sense. Then this linear combination serves as an updated set of initial conditions, called the "analysis", at t_{n+1} from which the model is integrated forward to the next time point t_{n+2}, and the above process is repeated. The mean of the analysis ensemble is used as the updated estimate of the "true" state of the system, and the sample covariance matrix represents the uncertainty in the analysis mean.

Since all computations below are done at time t_{n+1}, we drop the time dependence to simplify the notation. Let $\{\mathbf{x}_{b(k)}\}_{k=1}^{K}$ be the set of K state vectors that denote the background ensemble, where $\mathbf{x}_{b(k)} \in \mathbb{R}^m$, and let $\overline{\mathbf{x}}_b$ represent the corresponding ensemble mean. Let $\mathbf{X}_b$ be the $m \times k$ matrix whose kth column is $\mathbf{x}_{b(k)} - \overline{\mathbf{x}}_b$. Suppose that $\mathbf{w}$ is a Gaussian K-vector with mean $\mathbf{0}$ and covariance $(K-1)^{-1}\mathbf{I}$. Then $\mathbf{x} = \overline{\mathbf{x}}_b + \mathbf{X}_b\mathbf{w}$ has mean $\overline{x}_b$ and covariance $(K-1)\mathbf{X}_b\mathbf{X}_b^T$, which is the ensemble estimate of the model forecast uncertainty.

Let $\mathbf{y}^{\text{obs}}$ be the s-vector of observations, which is assumed to have the following relationship with the "true" model state vector $\mathbf{x_t}$ by

$$\mathbf{y}^{\text{obs}} = \mathbf{H}(\mathbf{x}_t) + \epsilon, \tag{4.1}$$

where ϵ is assumed to be an s-vector Gaussian error with mean $\mathbf{0}$ and covariance $\mathbf{R}$. The EnKF minimizes the cost function defined as

$$J(\mathbf{w}) = (K-1)\mathbf{w}^T\mathbf{w} + [\mathbf{y}^{\text{obs}} - \mathbf{H}(\overline{\mathbf{x}}_b + \mathbf{X}_b\mathbf{w})]^T\mathbf{R}^{-1}[\mathbf{y}^{\text{obs}} - \mathbf{H}(\overline{\mathbf{x}}_b + \mathbf{X}_b\mathbf{w})], \quad (4.2)$$

where the forward operator $\mathbf{H}$ is approximated as

$$\mathbf{H}(\overline{\mathbf{x}}_b + \mathbf{X}_b\mathbf{w}) \approx \overline{\mathbf{y}}_b + \mathbf{Y}_b\mathbf{w}. \quad (4.3)$$

Here $\overline{\mathbf{y}}_b$ is the mean of the background observation ensemble

$$\mathbf{y}_{b(k)} = \mathbf{H}(\mathbf{x}_{b(k)}), \quad k = 1, \ldots, K \quad (4.4)$$

and the kth column of the $s \times K$ matrix $\mathbf{Y}_b$ is $\mathbf{y}_{b(k)} - \overline{\mathbf{y}}_b$. The minimizer of Equation (4.2) is found in the form

$$\overline{\mathbf{w}}_a = \widetilde{\mathbf{P}}_a\mathbf{Y}_b^{\mathrm{T}}\mathbf{R}^{-1}(\mathbf{y}^{\text{obs}} - \overline{\mathbf{y}}_b) \quad (4.5)$$

$$\widetilde{\mathbf{P}}_a = \left[(k-1)\mathbf{I} + \mathbf{Y}_b^{\mathrm{T}}\mathbf{R}^{-1}\mathbf{Y}_b\right]^{-1}. \quad (4.6)$$

In model space, the analysis mean and covariance become, respectively

$$\overline{\mathbf{x}}_a = \overline{\mathbf{x}}_b + \mathbf{X}_b\overline{\mathbf{w}}_a \quad (4.7)$$

$$\mathbf{P}_a = \mathbf{X}_b\widetilde{\mathbf{P}}_a\mathbf{X}_b^{\mathrm{T}}. \quad (4.8)$$

As mentioned earlier, the analysis ensemble is derived from a linear combination of the background ensemble members. The first step in this procedure is to compute the symmetric square root

$$\mathbf{W}_a = \left[(k-1)\widetilde{\mathbf{P}}_a\right]^{1/2}. \quad (4.9)$$

The analysis ensemble $\{\mathbf{w}_{a(k)}\}_{k=1}^K$ is formed by adding $\overline{\mathbf{w}}_a$ to each column of $\mathbf{W}_a$. Then in model space, the analysis ensemble is

$$\mathbf{x}_{a(k)} = \overline{\mathbf{x}}_b + \mathbf{X}_b\mathbf{w}_{a(k)}, \quad k = 1, \ldots, K. \quad (4.10)$$

More details on the derivation of the EnKF are given in Hunt *et al.* (2007).

4.2.2 State Augmentation

In order to use the EnKF algorithm for a state-parameter estimation, an augmented state system that includes both the model variables and parameters is required. Let us rewrite the Model T-5, Equations (3.9-3.13), in the compact form

$$\frac{d\mathbf{x}}{dt} = F(t, \mathbf{x}), \tag{4.11}$$

where $\mathbf{x}$ is the m-dimensional model state vector. Let $\mathbf{p}$ be an n-dimensional vector of selected model parameter. Considering the $(m+n)$-dimensional state vector $\mathbf{x}^* = (\mathbf{x}, \mathbf{p})^T$, the EnKF can be used to solve the augmented system

$$\frac{d\mathbf{x}^*}{dt} = \begin{pmatrix} \frac{d\mathbf{x}}{dt} \\ \frac{d\mathbf{p}}{dt} \end{pmatrix} = \begin{pmatrix} \mathbf{F}(t, \mathbf{x}, \mathbf{p}) \\ \mathbf{G}(t, \mathbf{x}, \mathbf{p}) \end{pmatrix}, \tag{4.12}$$

where $\mathbf{G}$ is the model for the parameter space $\mathbf{p}$, which is assumed to be $\mathbf{G} = \mathbf{0}$. However, one can always choose a more complicated model for $\mathbf{G}$ rather than the simplest case considered here. The forward operator for the augmented system becomes $\mathbf{H}^* = (\mathbf{H}, \mathbf{0})^T$, because there is no observations for $\mathbf{p}$. Let $\tilde{\mathbf{F}} = (\mathbf{F}, \mathbf{G})^{\mathbf{T}}$ denote the augmented vector field. The forecast-and-update cycle can be presented in the following steps:

1. Set the previous analysis ensemble, $\{\mathbf{x}^n_{a(k)}\}^K_{k=1}$, as the initial conditions for the next short forecast.

2. Integrate the model $\tilde{F}(t, \mathbf{x}^*)$ from t_n to t_{n+1} for each ensemble member to obtain the background ensemble at time t_{n+1}: $\{\mathbf{x}^{n+1}_{b(k)}\}^K_{i=1}$.

3. Map the background ensemble to the observation space at time t_{n+1} by applying the forward operator $\mathbf{H}^*$ to each of the background ensemble member: $\mathbf{y}^{n+1}_{b(k)} = \mathbf{H}^* \left(\mathbf{x}^{n+1}_{b(k)}\right), k = 1, \ldots, K$.

4. Minimize the cost function, Equation (4.2), which produces the analysis at time t_{n+1}: $\{\mathbf{x}_{a(k)}^{n+1}\}_{k=1}^{K}$ with covariance matrix $\mathbf{P}_a^{n+1}$.

5. Use updated analysis ensemble $\{\mathbf{x}_{a(k)}^{n+1}\}_{k=1}^{K}$ as the initial conditions for the next background ensemble and repeat above steps.

4.3 Results and Discussion

The ensemble Kalman filter (EnKF) is useful to quantify the uncertainty in model predictions and parameters, provided that the latter are identifiable. As outlined in Section 4.2, the EnKF updates the model state vector in real time whenever new observations are available. The updated state vector is then used as the new initial condition for the next short forecast. In addition, an augmented state system, Equation (4.12), is implemented within the EnKF framework to update the chosen patient-specific parameters. In particular, these 3 parameters of Model T-5 are included in the augmented system: A_0, γ_1, and q_2. The other two parameters μ_m and d_1 are fixed at the same values as means of estimated parameters in Table 3.2 for all patients, because they do not vary significantly among the patients. Having a smaller set of parameters helps to reduce the prediction uncertainty (smaller ensemble variance), with all other factors held equal. However, as mentioned above, q_2 may be practically unidentifiable, so including this parameter to be estimated can be problematic, which will be discussed with specific results below.

The initialization of the ensemble (the first background ensemble) is another important factor to consider. The sample variance of the initial conditions is supposed to represent that of the underlying state space, but neither the initial proportion of treatment-sensitive cells nor the amount of intracellular androgen in each patient's tumor can be measured. Moreover, the uncertainty in patient-specific model parameters may be large, which cannot be known or measured beforehand. As a guess, 100

initial values of the initial state vector are chosen randomly from 0.7 to 1.6 times the value of each component of initial condition $\mathbf{x}_0$ estimated for each patient in Phan *et al.* (2019). The initial ensemble mean values of the parameters A_0, γ_1 and q_2 are provided by the output from MATLAB built-in function *fmincon* that minimizes the mean squared error of observations and model predictions, results seen as in Table 3.2. The standard errors for these 3 parameters are estimated from the respective 95% confidence intervals in Figure 4.1. Altogether, the augmented state vector becomes $\mathbf{x}^* = (x_1, \ldots, x_5, A_0, \gamma_1, q_2)^T$. The standard errors in the observations for serum PSA and androgen levels are assumed to be independent and have variance of 1.

The first background ensemble is obtained by integrating the initial conditions of the 100-member ensemble to the first observation time t_1, then the analysis ensemble is computed by minimizing the cost function Equation (4.2), which becomes the new initial condition for the next background ensemble. The integration continues to the second time step t_2 and the assimilation cycle is repeated until the end of the time series or until another predetermined ending time. We ran the EnKF algorithm for 26 patients chosen from the Vancouver Prostate Cancer database.

For each patient, we ran the EnKF in two different settings. In the first setting, the computational model only assimilates data from the first on-off-on treatment interval and continues with free model run (no data assimilation) for the subsequent off-on intervals using parameter values updated at the end of the first 1.5 treatment cycles. Three representative patient-specific results are shown in Figure 4.2, and the left panels are results for the first setting of model run. The ensemble mean is given by red curves, and the ensemble member solutions are shown as the gray curves. The black circles are patient's clinical data. The second setting is to run the EnKF through the entire time series of an individual patient, shown as the panels on the right in Figure 4.2. The first setting is used to assess the model's predictive ability

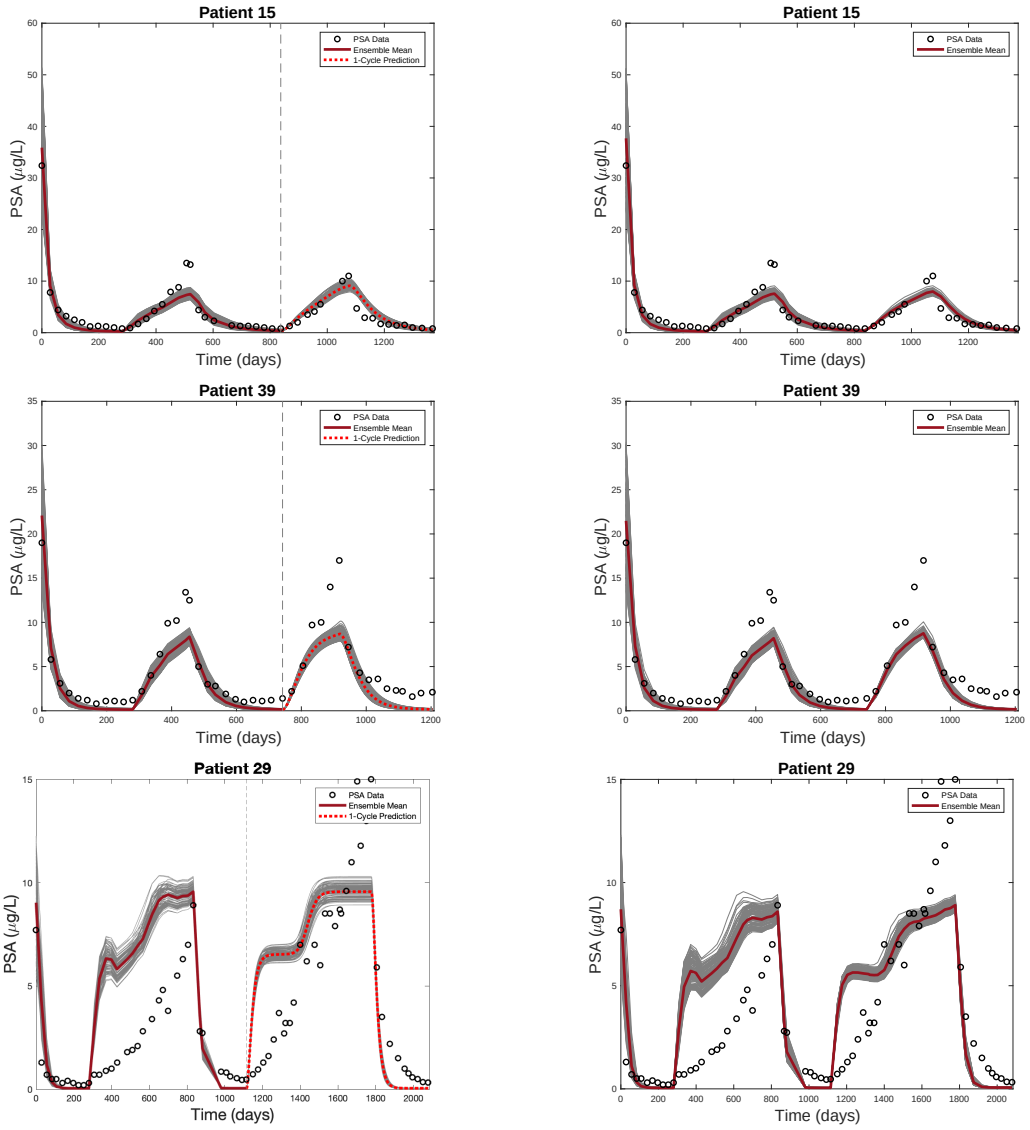

Figure 4.2: Representative ensemble Kalman filtering results of predicted PSA levels for three patients. Red curves: ensemble mean. Gray curves: ensemble member solutions. Black circles: clinical observations. For left panels, the vertical dashed line separates the 1.5 cycles of EnKF from the 1-cycle prediction. The right panels are results for the same patients but the EnKF is run through the entire time series.

and the second setting is used to gain more insights on the uncertainty in model predictions.

In order understand the uncertainty in model predictions, a simple metric is developed for results seen as the right panels in Figure 4.2. At each observation time t_n, the mean of the predicted PSA level from the analysis at t_{n-1} over all 100 ensemble members is given as

$$\overline{y}_n = \frac{1}{100} \sum_{k=1}^{100} \mathbf{H}(\mathbf{x}_{b(k)}(t_n)). \tag{4.13}$$

At the end of the time series, the root mean square (RMS) of the one-step ahead prediction error of serum PSA level averaged over all N observation time points is

$$\hat{P} = \left(\frac{1}{N} \sum_{n=1}^{N} \left(\overline{y}_n - y^{\text{obs}}(t_n) \right)^2 \right)^{1/2}. \tag{4.14}$$

The calculated $\hat{P}$ values for Patient 15, Patient 39, and Patient 29 are 1.80, 2.38, and 2.84 μg/L, respectively.

In the case of Patient 15, the EnKF update for PSA level is in good agreement with observations throughout the clinical time series. Viewing the left panel of Patient 15, during the first on-off-on interval, the ensemble mean underestimates the observed PSA levels towards the end of the first off-treatment cycle. However, prediction of another treatment cycle using parameters updated around day 800 (the last analysis) shows much improvement towards the end of the second off-treatment cycle. When the data assimilation cycle is halted shortly after day 800, the model provides a good prediction of the patient's treatment response over the next off- and on-treatment cycles. When the EnKF is run continuously throughout the entire clinical course of Patient 15, the variance in ensemble prediction decreases over time. As stated above, the RMS error of the ensemble mean's one-step ahead prediction of PSA level is about 1.80 μg/L.

The results for Patient 39 are similar, though the ensemble mean tends to underestimate the observed serum PSA levels towards the end of each on-treatment cycle. As with Patient 15, the augmented state vector produced by the EnKF at the end of the second on-treatment interval yields a reasonable 450-day prediction of Patient 39's clinical course.

However, results from Patient 29 shows serious problems in model predictions. In particular, during the off-treatment intervals, the ensemble forecasts show significant model errors. The filter is initialized the same way as for the other patients, but how can it perform so poorly for Patient 29? This problem is associated with the parameter estimation for q_2, the cell quota for the treatment-resistant tumor cell subpopulation. As shown in Figure 4.1, the profile likelihood of q_2 shows its 95% confidence interval includes values that are not biologically meaningful, which suggests that it may be unidentifiable with the given data.

Figure 4.3 shows the parameter estimations give by the EnKF for Patient 29. The blue curves give the range (minimum and maximum) of the ensemble estimations for the parameters A_0, γ_1, and q_2, and the green curve gives the ensemble mean. The biological assumption of Model T-5 is $q_1 > q_2$: the treatment-sensitive cell population requires more androgen to grow than the treatment-insensitive cell population. However, for Patient 29, some of the ensemble estimates for q_2 exceeds the fixed $q_1 = 0.613$. In this case, the model cannot be used to explain the observed dynamics. As shown in Figure 4.2, the forecast ensemble for Patient 29 diverges shortly from reality, and of course the model's predictions are not believable.

The last example is included as a cautionary note in the application of the ensemble Kalman filter. One needs to keep in mind that the patient-specific parameters being estimated have a sufficiently small variance so that the ensemble updates of these parameters can remain within a sensible range for the model under considera-

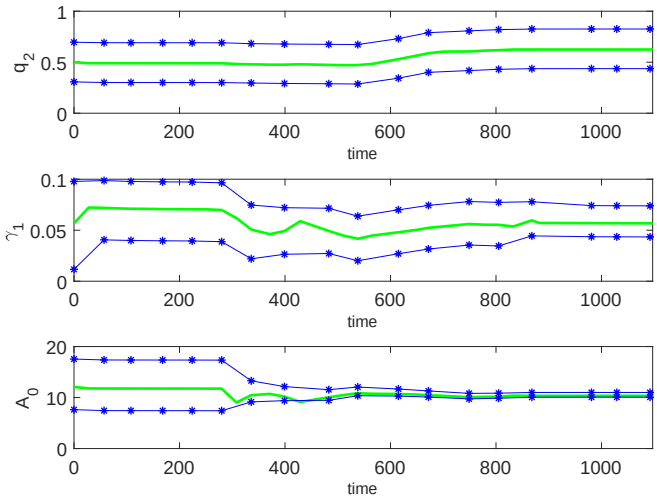

Figure 4.3: Augmented ensemble Kalman filter parameter estimates of Patient 29 from Model T-5. Green curve: ensemble mean; blue curves: minimum and maximum ensemble values.

tion. An alternative to cope with this challenge is to modify the EnKF framework by adding a suitable penalty term to Equation (4.2) to further constrain the parameter values, but the resulting optimization problem becomes nonlinear and is more costly to solve numerically.

4.4 Conclusions

In the past 20 years, numerous mathematical models have been developed to study the biological mechanism of prostate tumors with or without treatment. As seen in Chapter 3, these models often appear in the form of ordinary differential equations with a set of model parameters that describe the underlying mechanism. Although these model parameters can be used to explain the possible causes of the tumor dynamics, most of these parameters cannot be measured directly in clinical

settings. Consequently, the uncertainty in these model parameters are large, refer to the parameter ranges in Table 3.1. Wu *et al.* (2019) carried an analysis for model parameters of three models: Model H, Model P, and Model T, each of which has been validated with clinical data in Hirata *et al.* (2010); Portz *et al.* (2012); Phan *et al.* (2019). They discovered a common problem for these models called parameter identifiability.

Many existing mathematical models of prostate cancer treatment are proven unidentifiable in Wu *et al.* (2019), which implies that there are multiple sets of parameters that can be used to fit a given data set equally well. Nevertheless, good fitting does not guarantee good predictions seen as in Figure 3.1. This problem motivates us to look into uncertainty quantification for existing models so that a useful application can be provided to aid with real clinical practices.

Model T-5 originally developed by Phan *et al.* (2019) is used in this study to develop a useful clinical application. This model has 5 model variables and 5 control parameters, which is proven to be an identifiable model in Wu *et al.* (2019). With an identifiable model, it is possible to quantify the uncertainty in model predictions. Hence, a data assimilation framework is built for Model T-5 in order to estimate the chosen patient-specific parameters directly from a patient's clinical data.

The ensemble Kalman filter is a useful way to assess (validate) the model with real data and quantify uncertainties in short-term predictions. The EnKF provides a systematic and consistent framework for Model T-5 to assimilate clinical observations and calibrate the model in real time by estimating important parameters from the data. Short-term treatment response predicted by the model is reliable for most of the patients chosen from the Vancouver Prostate Center database.

An improved model of IAS therapy is needed. The EnKF result for Patient 29 reveals significant model bias. The assumption of the model is not capable of explain-

ing every possible situation of the tumor dynamics. In the case of Patient 29, the model seems to settle at a local equilibrium which is not physical. Systematic model biases (errors) can be accounted in EnKF schemes (Baek *et al.* (2006)), but it is not pursued in this study. Furthermore, the assumption that the tumor is divided into two cell subpopulations based on the nutrient-limiting theory should be examined further for special cases of prostate cancer. For later staged prostate cancer, other types of screening such as bone scan are used to provide more accurate assessment of a patient's tumor progress. In the case that the tumor transforms into a population that is independent from androgen, the existing model will not capture the true tumor dynamics.

The application of observing-system simulation experiments (OSSEs) could contribute to the development of clinically applicable dynamical models of prostate cancer treatment, and many other cancers. OSSEs have been widely used in numerical weather prediction to improve the model's performance. Broadly speaking, in an OSSE, synthetic data are assimilated into a high-dimensional dynamical model in order to assess measures like prediction accuracy (predictive ability) as a function of the accuracy, sparsity, and types of observations. A more detailed historical review can be found in Arnold, Jr. and Day (1986). One important application concerns "the potential improvements in climate analysis and weather prediction to be gained by augmenting the present atmospheric observing system with additional envisioned types of observations that do not yet exist" (Errico *et al.* (2013)). In the context of prostate cancer treatment, OSSEs might be useful to quantify uncertainties in parameter estimates from data with various noise levels or to assess the impact of a new or other tumor diagnostic on the prediction skills of an existing model. Such efforts may be necessary to develop clinically validated mathematical models to provide useful tools for physicians and patients.

Chapter 5

REDUCED-ORDER MODELING OF THE POLAR VORTEX

5.1 Introduction

The polar vortex in the Northern Hemisphere is a low-pressure area of cold air above the Arctic. It is kept in the polar region by the polar jet stream, a high-speed current of air that circles the Earth between the Arctic and mid-latitudes. The state of the polar vortex varies together with the state of polar jet stream. When the polar jet stream is weak, it meanders southward to the mid-latitudes and transports the cold Arctic air from the polar region to lower latitudes. During wintertime, weakening of the polar vortex can cause outbreaks of Arctic air in lower latitudes that affect winter/spring weather in many European and/or Northern American countries. Current forecasting and climate models, such as global prediction models (NCEP, ECMWF) and general circulation models (GCMs) (Balachandran *et al.* (1999)), provide dynamical models to study the stratospheric dynamics, but relevant simulations incur a high computational cost. To better understand the mechanism underlying the variation of Arctic polar vortex, a reduced-order model is necessary for studying the long-term dynamics of polar vortex.

Multiple atmospheric factors may perturb the stratospheric polar vortex. Two of the major factors have been proposed and studied by Holton and Mass (1976), Yoden (1987), Yoden (1990), and Ruzmaikin *et al.* (2003). They are the vertical gradient of radiative zonal flow and the initial amplitude of planetary waves. The vertical gradient of the zonal wind is associated with solar forcing that has both a seasonal cycle and an 11-year solar cycle. The initial amplitude of planetary waves

represents forcing from vertically propagating planetary waves. Considering the two driving forces, Ruzmaikin *et al.* (2003) have developed a simple dynamical model composed of three ordinary differential equations that describe a one-dimensional atmospheric system localized as one point in the stratosphere. The "Ruzmaikin model" is a highly truncated version of the Holton and Mass 1976 model (the "HM76" model) of stratospheric wave-zonal flow interactions. It is obtained by considering only one longitudinal and one latitudinal mode of the HM76 model, and fixing the vertical level to 25 km log-pressure height using finite differences. Although such a one-dimensional model cannot realistically describe the complicated stratospheric dynamics, it captures the essential mechanism of interactions between planetary waves and the zonal wind.

Ruzmaikin *et al.* (2003) refer to the vertical gradient of the zonal wind as the parameter Λ, and the initial amplitude of planetary waves as the parameter h, which are the only two control parameters for the Ruzmaikin model (all other parameters are fixed). In their study, $\Lambda(t)$ is a time-dependent parameter accounting both the seasonal variability and the 11-year solar cycle variability of solar radiation. The planetary wave amplitude $h(t)$ at the bottom boundary is also time-dependent and equivalent to the perturbation at ground level. Bifurcation studies on these two control parameters (Figures 2 and 3 in Ruzmaikin *et al.* (2003)) show that the system is bistable in some ranges of Λ and h.

The bistability behavior of the zonal wind is demonstrated as one unstable equilibrium state in the middle and two stable equilibrium states on the top and bottom branches of the bifurcation diagram, shown in Figure 5.1. The upper branch in the diagram corresponds to a high winter zonal wind speed and a stable polar vortex (fast jet stream), while the lower branch corresponds to a low winter wind speed and an unstable polar vortex (slow jet stream). During a year, the system switches from

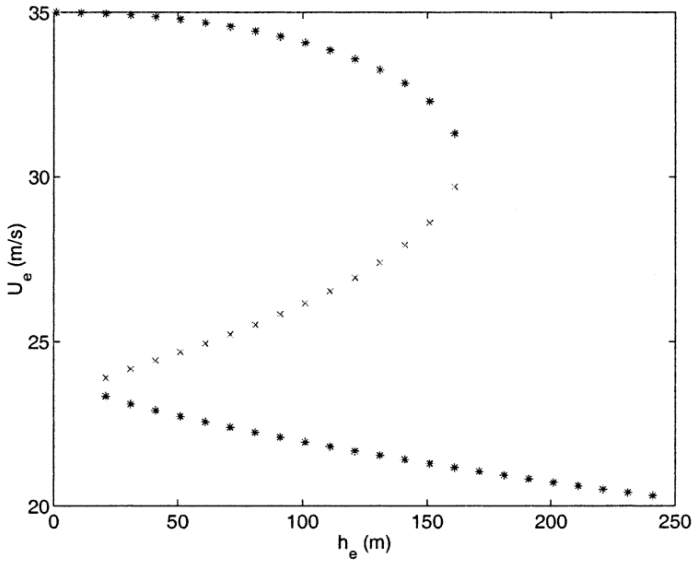

Figure 5.1: A bifurcation diagram of h, Figure 3 in Ruzmaikin *et al.* (2003) © American Meteorological Society. Used with permission. The crosses denote the unstable steady states, and the asterisks denote the stable steady states.

the single-well regime in the summer to the double-well regime in the winter. This double-well regime suggests an inherent uncertainty in predicting which branch the system will choose transitioning from autumn to winter each year.

Simulation of the model over the course of 25 years (refer to Figure 5.2) shows the temporal evolution of the polar jet stream: during winter time the zonal wind reaches its maximum of the year cycle; during summer time the wind changes direction and decreases to its negative minimum. Furthermore, this simulation also reveals the bistability behavior insofar as some winters exhibit a faster zonal wind of 80 m/s (stable polar vortex), while other winters exhibit a slower zonal wind around 30 m/s (unstable polar vortex). Despite the Ruzmaikin model being a simple one-dimensional model, it is able to capture the seasonal variability and inter-annual variability of the stratospheric dynamics. These qualitative behaviors studied by the model are also observed in the post-processed ECMWF reanalysis data shown in Figure 6.1.

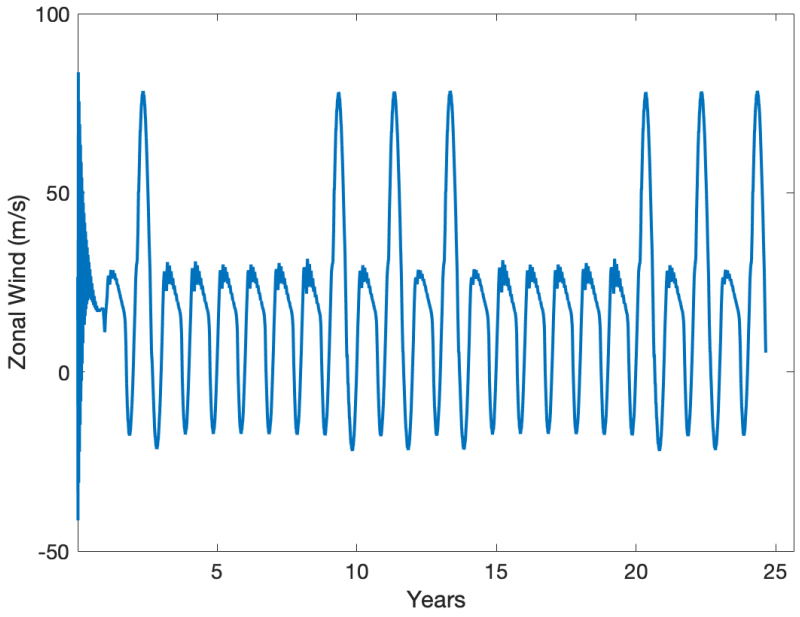

Figure 5.2: Simulation of zonal wind speed from the Ruzmaikin model with $\epsilon = 0.03, h = 68$.

The main purpose of the Ruzmaikin model is to study how perturbations from planetary waves and solar forcing could influence the state (stability) of the stratospheric polar vortex in long timescale of decades. This low-dimensional model provides an analytical tool to study the underlying mechanism of long-term dynamics of the Arctic polar vortex, which is too computationally expensive when simulated with global prediction and climate models. However, many model assumptions made by Ruzmaikin *et al.* (2003) to simplify a high-dimensional system may be oversimplifications of the dynamics and the physics pertinent to the polar vortex. For example, they have fixed h at 68 meters throughout their study so as to focus on studying the effect of solar forcing to the dynamics of the polar vortex. They assumed a constant forcing from vertically propagating planetary waves which is not realistic. It is uncertain that the assumptions of the Ruzmaikin model are representative of real

dynamics and physics. An assessment of this idealized model is necessary to answer this question.

The motivation of my study is to use data assimilation to assess the reduced-order model. In particular, I aim to develop a suitable data assimilation framework for the Ruzmaikin model to verify if the qualitative behavior of the zonal wind can be reproduced with the ECMWF reanalysis data under specific model assumptions. Furthermore, the control parameter h will be estimated directly from the reanalysis data using these two different model assumptions: h is constant and h is time-dependent. We want to search for evidences of bistability of the zonal flow associated with h from corresponding data assimilation results.

The analysis of the reduced-order model suggests that within certain range of the parameter h, there lies the bistable region of the zonal wind during winter time. However, this parameter has large uncertainty as shown in the bifurcation diagram that h can vary from zero to several hundred meters. No direct physical measurements of the wave amplitude are available to recover h. Thus, data assimilation can be used to estimate h directly under different model assumptions as proposed earlier. A sequential data assimilation scheme, the ensemble Kalman filter (EnKF), will be used to estimate a time-independent (constant) h. On the other hand, the ensemble smoother with multiple data assimilation (ES-MDA) will be used to estimate a time-varying h. The underlying mechanism of the polar vortex studied by the model: the bistable state of the polar vortex related to the vertical forcing from planetary waves, can then be validated with corresponding data assimilation updates of h and U.

In this chapter, the mathematical formulation of the Ruzmaikin model and relevant bifurcation studies for important model parameters will be discussed. The data assimilation application for this model and relevant results will be presented in Chapter 6.

5.2 Development of the Ruzmaikin Model

As mentioned above, the Ruzmaikin model represents a one-dimensional stratospheric system which includes prognostic equations for geostrophic streamfunction and zonal wind. This model is a simplified version of a mechanistic model of stratospheric wave-zonal flow interaction developed in Holton and Mass (1976) (the "HM76" model).

The HM76 model is a quasi-geostrophic $\beta-$plane channel model, which is similar to the one used by Geisler (1974) to study the essential dynamics of sudden stratospheric warming. Holton and Mass modified Geisler's model by adding a sine jet meridional variation to reflect the mean zonal flow's dependence on latitude, while Geisler assumed a zonal flow that is independent of latitude. This sine jet profile roughly models the observed polar night jet in the Northern Hemisphere and is associated with vertical forcing from planetary waves. HM76 assumes that the main driving forces of mean zonal circulation are differential radiative heating and horizontal eddy heat fluxes caused by vertically propagating planetary waves. The mean zonal wind $\overline{u}$ and the geostrophic streamfunction of a wave ψ' are assumed to take the following forms by Holton and Mass (1976):

$$\overline{u}(y,z,t) = U(z,t)\sin \ell y, \tag{5.1}$$

$$\psi'(x,y,z,t) = \mathrm{Re}[\Psi(z,t)e^{ikx}]e^{z/2H}\sin \ell y, \tag{5.2}$$

where k, ℓ are wavenumbers for x, y the standard azimuthal and latitudinal coordinates. Here f_0 is the Coriolis parameter at 60°N ($f_0 = 1.26 \times 10^{-4}\mathrm{s}^{-2}$) and H is a mean scale height ($H = 7$ km). Notice that the variable Ψ is complex valued. Holton and Mass also further assumed that the wave fields are governed by the linearized

quasi-geostrophic potential vorticity equation in log pressure coordinates:

$$\left(\frac{\partial}{\partial t}+\overline{u}\frac{\partial}{\partial x}\right)q'+\beta'\frac{\partial\psi'}{\partial x}+\frac{f_0^2}{\rho}\frac{\partial}{\partial z}\left(\frac{\alpha\rho}{N^2}\frac{\partial\psi'}{\partial z}\right)=0, \tag{5.3}$$

where

$$q'=\nabla^2\psi'+\frac{f_0^2}{\rho}\frac{\partial}{\partial z}\left(\frac{\rho}{N^2}\frac{\partial\psi'}{\partial z}\right) \tag{5.4}$$

represents the perturbation potential vorticity and

$$\beta'=\beta-\frac{\partial^2\overline{u}}{\partial y^2}-\frac{f_0^2}{\rho}\frac{\partial}{\partial z}\left(\frac{\rho}{N^2}\frac{\partial\overline{u}}{\partial z}\right) \tag{5.5}$$

represents the gradient of the basic state potential vorticity. Here β is the meridional derivative of the Coriolis parameter at 60°N which is $1.14\times10^{-11}\mathrm{s}^{-1}\mathrm{m}^{-1}$, N^2 is the buoyancy parameter fixed at $N^2=4\times10^{-4}\mathrm{s}^{-2}$, $\rho=\rho_0\times\exp(-z/H)$ is a standard density, and $\alpha=\alpha(z)$ is a Newtonian cooling rate coefficient.

The prognostic equation of the mean zonal flow is given by Holton and Mass (1976):

$$\frac{\partial}{\partial t}\left[\frac{\partial^2\overline{u}}{\partial y^2}+\frac{f_0^2}{N^2}\frac{1}{\rho}\frac{\partial}{\partial z}\left(\rho\frac{\partial\overline{u}}{\partial z}\right)\right]=-\frac{f_0^2}{N^2}\frac{1}{\rho}\frac{\partial}{\partial z}\left[\alpha\rho\frac{\partial(\overline{u}-u_R)}{\partial z}\right]+\frac{f_0^2}{N^2}\frac{\partial^2}{\partial y^2}\left[\frac{1}{\rho}\frac{\partial}{\partial z}\left(\rho v'\frac{\partial\psi'}{\partial z}\right)\right], \tag{5.6}$$

where $v'=\partial\psi'/\partial x$ and $\overline{u}$ is the mean zonal flow obtained by averaging over x. The flow is assumed to be confined to a $\beta-$channel centered at 60°N with a meridional extent L of 60° latitude. We substitute the assumed form of solutions, Equations (5.1) and (5.2), for ψ' and $\overline{u}$ into Equations (5.3) and (5.6). Then, the linearized quasi-geostrophic potential vorticity equation and mean-flow equation become, respectively

$$\begin{aligned}\left(\frac{\partial}{\partial t}+ik\epsilon U\right)\left[-(k^2+\ell^2)+\frac{f_0^2}{N^2}\left(\frac{\partial^2}{\partial z^2}-\frac{1}{4H^2}\right)\right]\Psi+\beta'_e ik\Psi\\ +\frac{f_0^2}{N^2}\left(\frac{\partial}{\partial z}-\frac{1}{2H}\right)\left[\alpha\left(\frac{\partial}{\partial z}+\frac{1}{2H}\right)\Psi\right]=0,\end{aligned} \tag{5.7}$$

$$\frac{1}{\epsilon}\frac{\partial\beta'_e}{\partial t}=\frac{f_0^2}{N^2}\left(\frac{\partial}{\partial z}-\frac{1}{H}\right)\left[\alpha\left(\frac{\partial U}{\partial z}-\frac{dU_R}{dz}\right)\right]+\frac{1}{2}k\ell^2\epsilon\frac{f_0^2}{N^2}e^{z/H}\mathrm{Im}\left[\Psi^*\frac{\partial^2\Psi}{\partial z^2}\right], \tag{5.8}$$

where

$$\beta_e' = \beta + \ell^2 \epsilon U - \epsilon \frac{f_0^2}{N^2} \left(\frac{\partial^2 U}{\partial z^2} - \frac{1}{H} \frac{\partial U}{\partial z} \right). \tag{5.9}$$

A constant $\epsilon = 8/(3\pi)$ is derived from the truncation of nonlinear term $\sin^2 \ell y$ using Fourier sine series. With the specific localization of the $\beta-$channel, $\ell = 3/a = 4.71 \times 10^{-7}\mathrm{m}^{-1}$ and $k = 2/(a \cos \pi/3) = 6.28 \times 10^{-7}\mathrm{m}^{-1}$ where a is the earth radius. For the boundary conditions, HM76 assumes zero normal flow across the lateral boundaries which requires that ψ' and v' vanish at the side boundary $y = 0, L$. The upper and bottom boundaries are chosen at $z_B = 10$ km (tropopause) and $z_T = 80$ km (mesopause), respectively. The HM76 model assumes that perturbation and zonal mean flow vanish at the upper boundary and specifies the lower boundary conditions by setting $\overline{u} = \overline{u}_B(y)$ and $\psi' = \psi_B(y, t)$.

HM76 has two important parameters: mean zonal wind in radiative equilibrium $U_R(z, t)$ and wave amplitude at the bottom boundary $h(t)$. The latter governs the geopotential height perturbation:

$$\Psi(z_B, t) = \frac{g}{f_0} h(t), \tag{5.10}$$

at the lower boundary caused by forcing from upward propagating planetary waves. Holton and Mass were interested in studying the stratospheric response to vertically propagating planetary waves excited by steady tropospheric forcing. Hence, they fixed the radiative equilibrium zonal wind shear $\partial U_R/\partial z = 3$ m s^{-1}km^{-1} but defined a time dependent wave amplitude at the bottom boundary

$$h(t) = h_B[1 - e^{-t/\tau}].$$

Here $\tau = 2.5 \times 10^5$s and h_B is a specified parameter chosen by Holton and Mass to represent the asymptotic steady-state amplitude of the forcing.

Yoden then developed a simplified version of HM76 in 1987 and 1990 (Yoden (1987, 1990)), denoted as "Y87" and "Y90" hereafter. Y87 simplifies HM76 by using

central finite differencing for Ψ and U:

$$\left.\frac{\partial \Psi}{\partial z}\right|_{z=j\Delta z} = \frac{\Psi_{j+1} - \Psi_{j-1}}{2\Delta z}, \tag{5.11}$$

$$\left.\frac{\partial^2 \Psi}{\partial z^2}\right|_{z=j\Delta z} = \frac{\Psi_{j+1} - 2\Psi_j + \Psi_{j-1}}{\Delta z^2}, \tag{5.12}$$

where $j = 0, 1, \cdots, 28$ and similar expressions hold for derivatives of U. Applying this finite differencing, Y87 reduces Equations (5.7) and (5.8) to 81 nonlinear ordinary differential equations. Y87 changes the bottom boundary to 0 km instead of the tropopause as in HM76 and specifies the top and bottom boundary conditions as:

$$\Psi(z_T, t) = 0, \tag{5.13}$$

$$\left.\frac{\partial U}{\partial z}\right|_{z=z_T} = \left.\frac{dU_R}{dz}\right|_{z=z_T}, \tag{5.14}$$

$$\Psi(0, t) = g h_B(t)/f_0, \tag{5.15}$$

$$U(0, t) = U_R(0), \tag{5.16}$$

where h_B plays the same role as $h(t)$ in HM76 but is assumed to be constant in Yoden's studies. For the radiative equilibrium U_R, Y87 uses the same simple linear model suggested by Holton and Dunkerton (1978):

$$U_R(z, t) = U_{RB} + \Lambda(t) z, \tag{5.17}$$

where Yoden fixed U_{RB} at 10 m s^{-1} and Λ at 2 m s^{-1}/km. Hence dU_R/dz is assumed to be constant by Y87. Yoden used Y87 to study how vertical wave forcing affects the zonal circulation. Thus, he carried a bifurcation study on the parameter h_B and showed that there exists a multiplicity of stable steady solutions within certain ranges of h_B.

Y90 is identical to the form of Y87 but assumes time dependency in dU_R/dz by adding an annual component with the following form:

$$\frac{dU_R}{dz}(t) = 0.75 - 2.25 \cos\left(\frac{2\pi t}{365}\right), \tag{5.18}$$

where time t is expressed in day. Y90 illustrates the seasonal variation of the stratospheric circulation by adapting the periodic radiative heating.

Ruzmaikin *et al.* (2003) further simplified Y87 and Y90 by using finite differences in a single layer for Equations (5.11) and (5.12). They considered $j = 0, 1, 2$ in the finite difference scheme and used variables defined at the middle height $z_T/2$ with $\Delta z = z_T/2$ (z_T is assumed to be 50 km here). Boundary conditions are taken into account at the top and bottom. This produces the approximation:

$$\frac{\partial \Psi}{\partial z} = \frac{\Psi_2 - \Psi_0}{2\Delta z} = -\frac{gh}{f_0 z_T}, \tag{5.19}$$

$$\frac{\partial^2 \Psi}{\partial z^2} = \frac{\Psi_2 - 2\Psi_1 + \Psi_0}{\Delta z^2} = -\frac{8\Psi}{z_T^2} + \frac{4gh}{f_0 z_T^2}, \tag{5.20}$$

$$\frac{\partial U}{\partial z} = \frac{U_2 - U_0}{2\Delta z} = \frac{U_1 - U_R(0) + \Lambda z_T/2}{z_T}, \tag{5.21}$$

$$\frac{\partial^2 U}{\partial z^2} = \frac{U_2 - 2U_1 + U_0}{\Delta z^2} = -\frac{4(U_1 - U_R(0) - \Lambda z_T/2)}{z_T^2}. \tag{5.22}$$

This reduction of Yoden's 81 ordinary differential equations removes the vertical dependence. Rewrite $\Psi = X(t) + iY(t)$ and substitute Equations (5.19 - 5.22) back to the linearized quasi-geostrophic potential vorticity equation and zonal wind prediction equation. Then, the Ruzmaikin model appears in the final form of three ordinary differential equations:

$$\dot{X} = -X/\tau_1 - rY + sUY - \xi\Psi_0 + \delta_w \dot{\Psi}_0, \tag{5.23}$$

$$\dot{Y} = -Y/\tau_1 - rX + sUX + \zeta\Psi_0 U, \tag{5.24}$$

$$\dot{U} = -(U - U_R)/\tau_2 - \eta\Psi_0 Y - \delta_\Lambda \dot{\Lambda}, \tag{5.25}$$

where $U_R = U_R(z_T/2) = U_R(0) - \Lambda z_T/2$. The appendix of Ruzmaikin *et al.* (2003) gives the derivation of all other fixed parameters.

The two control parameters of this model are the same as HM76, Y87, and Y90: $\Psi(0,t) = gh(t)/f_0$ and $\Lambda(t) = dU_R/dz$. The overdot of these two parameters in

Equations (5.23) and (5.25) represents the corresponding time derivative. Ruzmaikin *et al.* (2003) used a contant h throughout their study and hence $\dot{\Psi}_0 = 0$ in this case. In their study, they modified the gradient of the mean radiative zonal wind by adding a solar cycle component to the periodic form obtained in Y90:

$$\Lambda(t) = \frac{dU_R}{dz}(t) = \Lambda_0 + \delta\Lambda_a \sin\left(\frac{2\pi t}{1 \text{ yr}}\right) + \delta\Lambda_s \sin^2\left(\frac{\pi t}{11 \text{ yr}}\right), \tag{5.26}$$

where $\Lambda_0 = 0.75, \delta\Lambda_a = 2.25$ and $\delta\Lambda_s = \epsilon\Lambda_0$ with $0 \leq \epsilon \leq 0.3$. Ruzmaikin *et al.* (2003) varied ϵ to control forcing from the 11-year solar cycle, which shows inter-annual variability in the long-term simulations of the model. Figure 5.3 reproduces Figure 4 in Ruzmaikin *et al.* (2003), which shows both seasonal and inter-annual variations in stratospheric circulations. Notice that the simulated zonal wind speeds are not identical to the results in Ruzmaikin *et al.* (2003), because the initial conditions are chosen differently.

The Ruzmaikin model is the final product of continuous modeling efforts originated from the HM76 model of stratospheric wave-mean flow interaction. A linearized quasi-geostrophic potential vorticity equation and the Holton-Mass zonal flow prediction equation are used as the prognostic equations for the wave-flow interaction in stratosphere. The Ruzmaikin model is localized to a $\beta-$channel centered at 60°N with meridional extent of 60° and vertical level of 25 km log pressure height. Important model parameters are the vertical gradient of the zonal wind $\Lambda(t)$ and the initial amplitude of planetary waves $h(t)$. These two parameters are described differently by HM76, Y87, Y90, and the Ruzmaikin model to study the stratospheric response to various forms of perturbations. In particular, Ruzmaikin *et al.* (2003) focused on studying the effect of weak solar forcing to the stratosphere and assumed seasonal and 11-year solar cycles for the parameter $\Lambda(t)$. Although $h(t)$ is defined as time-dependent, Ruzmaikin *et al.* (2003) fixed this parameter at 68 meters throughout

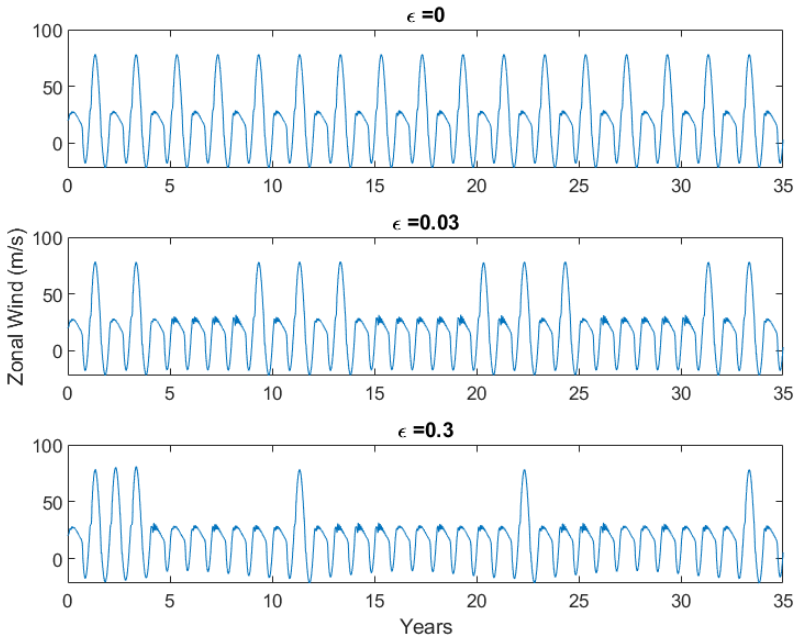

Figure 5.3: Multiple model runs of the Ruzmaikin model with different choices of $\epsilon = 0, 0.03, 0.3$ from top to bottom, respectively. Fixed h at 68 m. Plotted zonal wind over 35 years.

their study. The Ruzmaikin model indicates the seasonal and inter-annual variations of the stratospheric circulation.

5.3 Bistability Analysis of the Ruzmaikin Model

The two control parameters of the Ruzmaikin model are the initial wave amplitude $h(t) = f_0\Psi(0,t)/g$, and the vertical gradient of mean radiative zonal wind $\Lambda(t) = dU_R/dz$. Notice that h is equivalent to the amplitude of the wave perturbation $\Psi(0,t)$ at the ground level. However, Ruzmaikin *et al.* (2003) used a constant wave perturbation h at $z = 0$ m to study only the perturbation from solar forcing to the upper stratosphere. They treated h as a statistical winter mean value that is independent of the low-frequencies in the stratosphere.

While h is fixed, Ruzmaikin *et al.* (2003) assumed a time-dependent Λ with the functional form in Equation (5.26). This form of $\Lambda(t)$ includes a one-year seasonal cycle and an 11-year solar cycle. The magnitudes of the seasonal variation and the inter-annual variation (caused by solar cycle) are controlled by the parameters $\delta\Lambda_a$ and $\delta\Lambda_s = \epsilon\Lambda_0$, respectively. In their study, they chose ϵ out of the range $0 - 0.3$ to study the long-term effect of solar cycle forcing onto the zonal flow, shown in Figure 4 in Ruzmaikin *et al.* (2003). Their numerical experiments verified the bistable state of zonal wind with different values of Λ. Furthermore, they carried a bifurcation analysis on Λ and discovered a bistable region of U depending on specific values of Λ (while h is fixed), shown in Figure 3 in Ruzmaikin *et al.* (2003).

Similarly, through a bifurcation analysis, Ruzmaikin *et al.* (2003) confirmed the importance of the specific value of h to the equilibrium value of U, as illustrated in Figure 5.1. In particular, the model admits a wide range of values of h that recovers the bistability of the system. Small values of h are associated with less planetary wave interference with the polar jet and therefore fast zonal winds at equilibrium and a stable polar vortex. This case is equivalent to the upper stable branch in the bifurcation diagram. On the other hand, large values of h correspond to more intense forcing from planetary waves which therefore cause the jet stream to weaken, as seen by slower equilibrium zonal wind. This situation is realized by the bottom stable branch in the bifurcation diagram. Between these two extremes, however, lies a region with two stable branches corresponding to each of these polar jet behaviors. Thus, they choose an $h = 68$ m well within this region to exhibit the multiple states of the polar jet when investigating time-dependence via the parameter $\Lambda(t)$.

Following the assumption made by Ruzmaikin *et al.* that h is time-independent, I choose 100 values of h randomly from the range $50 - 100$ m to simulate the Ruzmaikin model. Figure 5.4 shows wide spread values of zonal wind predictions (especially

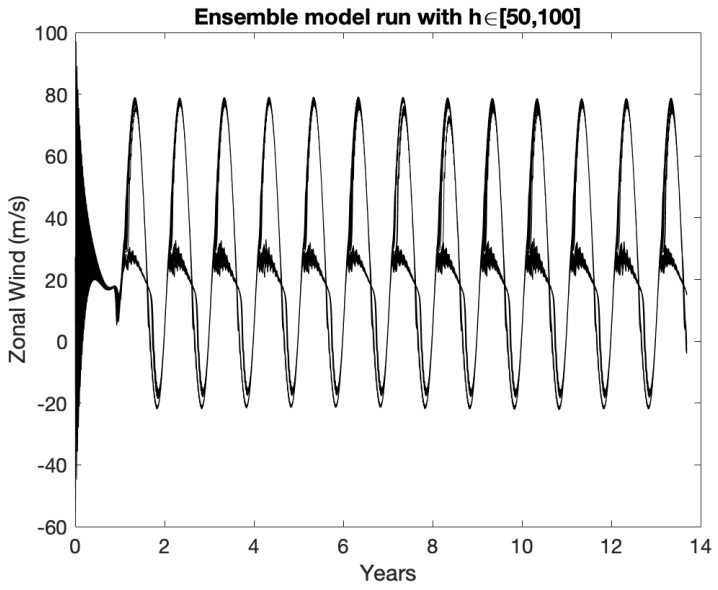

Figure 5.4: 100 ensemble simulations of the Ruzmaikin model with values of h chosen in the range $[50, 100]$ m. Zonal flow is plotted against time for each choice of h. All ensemble members are initialized with the same initial condition of X, Y, U and $\epsilon = 0.03$.

during wintertime) among the 100 ensemble members. The bistable state of the system is validated by the results shown in this figure as every winter both stable branches of the zonal wind in Figure 5.1 are simulated by ensemble predictions. Figure 5.5 shows zonal wind predictions from three individual ensemble members chosen from the previous ensemble run. These three model runs are initialized with different values of h (values are indicated on the top of the panels shown) within the bistability region and thus also validate the bifurcation analysis of h in Ruzmaikin *et al.* (2003).

5.4 Uncertainty Quantification for the Parameter h

The numerical experiments with h from the previous section implies that the stratospheric circulation is sensitive to the forcing driven by planetary waves. The amplitude of planetary waves h is an important model parameter to study and un-

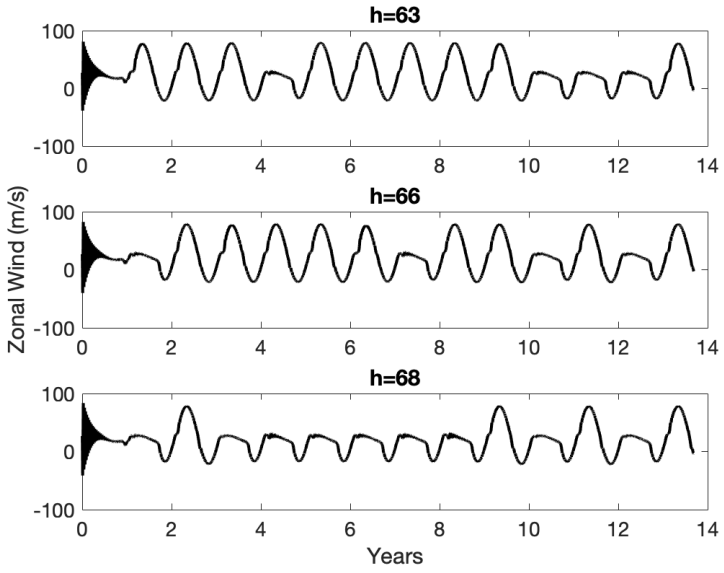

Figure 5.5: Three individual ensemble members chosen from the 100 ensemble predictions of zonal wind from Figure 5.4, corresponding to particular choices of h as indicated.

derstand the bistability behavior of the polar vortex. In contrast to the other control parameter Λ, which has tractable forms to explain the dynamics, h is a highly uncertain parameter. The planetary waves are forced by topography and sea-land contrasts in the Northern Hemisphere. According to Ruzmaikin *et al.* (2003), h could vary from zero to several hundred meters. They assumed that h is constant and equals to 68 meters throughout their study to focus only on the effect of solar forcing to the stratospheric circulation.

On the other hand, time-dependent h has also been suggested by various scholars. Holton and Mass (1976) used a exponential function of h in the form

$$h(t) = h_B(1 - e^{-t/\tau}), \tag{5.27}$$

where h_B is the asymptotic steady-state amplitude of the forcing and $\tau = 2.5 \times 10^5$ s. They chose h_B arbitrarily to study wave-mean flow oscillations caused by tropospheric

forcing. Yoden (1990) used a periodic form of h:

$$h(t) = 130 + 30\cos\omega_i t, \tag{5.28}$$

where t is in days and $0.0459\ \text{day}^{-1} \leq \omega_i \leq 0.0823\ \text{day}^{-1}$. He used this form of h to examine the effect of intraseasonal variations of wave forcing from the troposphere. Hu and Tung (2002) performed Fourier analysis for the observational data provided by NCEP (National Center for Atmospheric Research) and also demonstrated the time dependency of h, shown in Figures 1 and 2 in Hu and Tung (2002).

Previous studies of h show poor predictability in this parameter (Holton and Mass (1976); Yoden (1990); Hu and Tung (2002); Ruzmaikin *et al.* (2003)). Moreover, direct physical observations (meteorological data) are not available for amplitude of planetary waves to provide estimates for h. In order to assess the qualitative behaviors of the Ruzmaikin model with real data (available observations for model variables), it is necessary to obtain estimates of h that are consistent with the observed data. Data assimilation could be helpful to give insights for the uncertain model parameter h, because it provides a computational model to recover (infer) the "true" values of h directly from the data.

Furthermore, different assumptions of the time-dependency of h can be explored with suitable data assimilation frameworks such as ensemble Kalman filter (EnKF) or ensemble smoother. To investigate the assumption made by Ruzmaikin *et al.* (2003) that h is constant over time, the EnKF will be used to provide a state-parameter estimation framework for the Ruzmaikin model. This is a sequential data assimilation scheme that provides predictions of the model state and the time-independent h simultaneously. Alternatively, the ensemble smoother with multiple data assimilation (ES-MDA) will be used to test the other assumption that h is time-dependent. ES-MDA is a global data assimilation scheme which assimilates all historical data at

once and iterates the data assimilation cycles until optimal parameters are found. Ensemble smoothers can be viewed as solving a history-matching problem to look for the true parameters that reflect the history. ES-MDA only updates the parameter space of a model.

For both data assimilation schemes, the same data set obtained from the ERA-Interim archive provided by the ECMWF Reanalysis is used to study the time-dependency of h. The data set is averaged according to the assumption of model levels: 25 km log-pressure height and β-channel centered at 60°N. The main purpose of developing these data assimilation applications for the Ruzmaikin model is to validate the qualitative behaviors of the model, specifically, the inter-annual variations of the zonal wind associated with planetary wave perturbations (the bistability of zonal wind). Although this reduced-order model serves as a mechanistic model of a complex system of the polar vortex, it is inevitable to encounter model bias as a result of crude representation of real dynamics and physics. Hence, assessment and validation of the reduced-order model using data assimilation can provide insights for possible model errors and thereafter improve the model performance to better reflect the observed dynamics.

Chapter 6

DATA ASSIMILATION WITH A REDUCED-ORDER MODEL OF THE ARCTIC POLAR VORTEX

6.1 Introduction

Chapter 5 presented a reduced-order model of the Arctic polar vortex developed by Ruzmaikin *et al.* (2003), which is referred as the "Ruzmaikin model". As stated in the previous chapter, the Ruzmaikin model is a highly truncated version of the original PDE (partial differential equation) model developed in Holton and Mass (1976) to study stratospheric wave-zonal flow interactions. The final form of the Ruzmaikin model is a set of three ordinary differential equations that describe a one-dimensional stratospheric dynamical system.

Two important control parameters of the Ruzmaikin model are: Λ, the vertical gradient of zonal wind associated with solar forcing, and h, the initial amplitude of planetary waves at the bottom level. Time dependency are assumed for both parameters. However, for simplicity, Ruzmaikin *et al.* (2003) fixed $h = 68$ m in their study to focus only on the effect of weak solar forcing to the stratosphere circulation. The parameter Λ is defined as a periodic function accounting an annual cycle and an 11-year solar cycle of solar forcing. Ruzmaikin *et al.* (2003) have shown the bistability of zonal wind recovered by the parameter Λ both analytically and numerically, shown in Figures 2 and 4 in Ruzmaikin *et al.* (2003). Similarly, they have also done a bifurcation analysis for the other control parameter h to show that there is bistability of the system recovered by some range of h values as well, seen as in Figure 3 of Ruzmaikin *et al.* (2003). I performed some numerical simulations of the Ruzmaikin

model with different values of h and was able to verify the bistability behavior studied by the model, refer to Figures 5.4 and 5.5.

After a thorough literature review for the control parameter h (Holton and Mass (1976); Yoden (1990); Hu and Tung (2002); Ruzmaikin *et al.* (2003)), I realized that h has large variability and uncertainty. Well developed theories or direct physical measurements are not available to provide accurate estimates for h. Instead, data assimilation is applied to develop a useful computational application for the Ruzmaikin model so that h can be estimated directly from available data to verify the model's qualitative properties related to h.

In this chapter, the main goal is to develop suitable data assimilation methods to test different assumptions about h and validate the qualitative properties of the model. In particular, a time-independent h (a constant h) can be estimated via the ensemble Kalman filter (EnKF) with an augmented state vector. Alternatively, a time-varying h can be estimated using a global data assimilation scheme called the ensemble smoother with multiple data assimilation (ES-MDA). The updates for h and U given by specific data assimilation frameworks provide evidences to verify the bistability of the wind sown in Figure 5.1.

To assess the Ruzmaikin model, twenty years (1999 to 2018) of zonal wind data are obtained from ECMWF Reanalysis - Interim (or "ERA-Interim"), a global atmospheric reanalysis available from 1979. The reanalysis is based on a 2006 release of the ECWMF's Integrated Forecast System (IFS). The data assimilation system of ERA-Interim uses a 4-dimensional variational analysis (4D-Var) with a 12-hour analysis window. More details of the ERA-Interim archive can be found in Berrisford *et al.* (2011). We averaged the data set according to the assumptions of the Ruzmaikin model: the vertical level is fixed at 25 km log-pressure height, and the latitudinal channel is centered at 60°N. Both data assimilation schemes assimilate the reanalysis

data into the low-dimensional model under different model assumptions and generate parameter estimations for h. Results from these two different data assimilation schemes are compared and discussed in this chapter.

6.2 Data

6.2.1 Observations for the Zonal Wind

The zonal wind of the model (model variable U) is equivalent to "U component of wind" provided by ECMWF Reanalysis - Interim archive. Thus, twenty years (from 1999 to 2018) of U component of wind data are obtained from ECMWF Reanalysis. The data are selected at the pressure levels of 20 mb and 30 mb and grid resolution of $1^\circ \times 1^\circ$. Ruzmaikin *et al.* (2003) reduced the model to 25 km in log-pressure coordinate for the vertical level, which is between the pressure levels 20 mb and 30 mb. I used these two pressure levels to interpolate the data to 25 km log-pressure height by linear approximation in log-pressure vertical coordinate. In terms of time intervals, the data are selected from daily data with four time steps stored per day. The data are averaged over the four time steps each day to obtain daily averages of the zonal wind. Thus, the processed data set provides zonal wind "observations" as daily averages of the wind for each day, from 1 January 1999 to 31 December 2018.

The Ruzmaikin model is confined to a latitudinal channel centered at 60°N with a meridional extent of 60° latitude, so the daily means of zonal wind are then averaged over a latitudinal window centered at 60°N with meridional extents varying from 10° to 60° latitude. Different latitudinal channels are chosen to compare the variability of the data with respect to the window sizes. In Figure 6.1, the post-processed zonal wind data over different latitudinal windows are plotted, which illustrates that the smaller the window, the larger the variation of winter winds (relative maxima

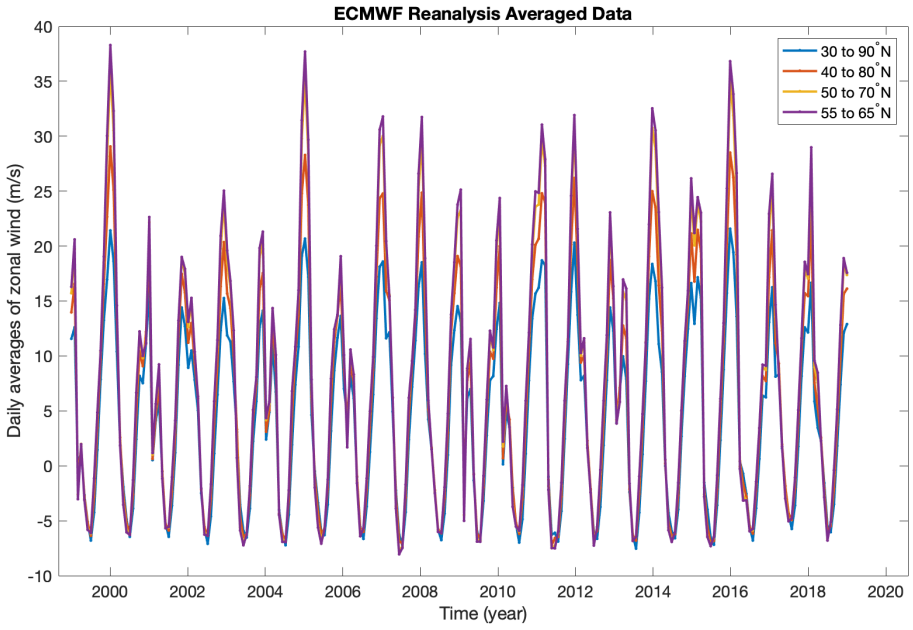

Figure 6.1: Daily averages of the ECMWF Reanalysis zonal wind data over different latitudinal windows centered at 60°N from year 1999 to 2018. The four sizes of the latitudinal window are $55-65$°N, $50-70$°N, $40-80$°N, and $30-90$°N.

and minima in the wind data). Though the magnitude of winter wind speed varies according to the window sizes, the bistability pattern of the wind is recovered by all window sizes.

6.2.2 Prior Estimate for a Time-dependent h: Geopotential Height

Parameter h is the amplitude of planetary waves at the lower boundary. It was fixed in Ruzmaikin *et al.* (2003) at $h = 68$ m. However, h acts as the perturbation to the polar jet and was proven to have time dependency by Hu and Tung (2002). They used geopotential heights from NCEP-NCAR reanalysis data to approximate for h. Similarly, in my study, the geopotential heights from ECMWF reanalysis data are used to provide time-dependent prior estimates of h for initialization of the ensemble.

Ruzmaikin *et al.* (2003) defined the lower boundary at the ground level, $z = 0$ m in log-pressure coordinates which is approximately at the pressure level of 1000 mb. This pressure level is close to the earth's surface and introduces complications related to extrapolation below the ground in the presence of elevated topography. For example, the extrapolation may cause negative values of the geopotential height at levels below the mountaintop as seen by the global model. Negative values for the geopotential height are not practical to approximate the amplitude of planetary waves, so a different pressure level of 500 mb is chosen instead. This level is located in the middle troposphere, well above any mountaintop, and captures upward propagating waves reaching the middle troposphere. All the four time steps of daily data are downloaded and averaged daily to provide daily means of geopotential heights.

To extract the wave amplitudes, Fourier analysis of geopotential height data was performed in a similar manner as in Hu and Tung (2002). Amplitudes of wave numbers 1 or 2 (depends on which wave number produces larger amplitude) are taken as the prior for time-varying h to initialize the ES-MDA algorithm.

6.3 Data Assimilation Methods for Parameter Estimation of h

Two different data assimilation methods are used to estimate h under different assumptions. First, following the assumption made by Ruzmaikin *et al.* (2003) that h is constant, the EnKF is applied to update the model state and the parameter simultaneously via an augmented state vector. We assume that $dh/dt = 0$ in the data assimilation framework. The augmented state is a concatenated vector that includes the three-dimensional model state and the parameter h. The EnKF will update h and the model state in real-time by calculating the error statistics (covariance matrix) of the ensemble forecast.

On the other hand, time-dependent values of h can be estimated using the ES-MDA. The ES-MDA is also an ensemble method but in contrast to the EnKF, it updates only the parameter space. In this study, eight parameters (including h) of the Ruzmaikin model are chosen to be updated by ES-MDA. Notice that the dimension of the parameter space is much larger than eight dimensions because h is assumed to be time dependent. Since daily means of the zonal wind are assimilated into the computation model, $h(t)$ is also updated daily which has a dimension of ~ 8000 corresponding to the 20 years of data.

6.3.1 The Ensemble Kalman Filter

The ensemble Kalman filter (EnKF) is a common sequential data assimilation scheme that can be used to estimate the state vector of a dynamical model given a set of noisy observations (Evensen (1994)). It is an iterative approach of the two steps: background forecast and analysis update. This type of sequential data assimilation scheme is useful for high-dimensional and nonlinear inverse problems.

The EnKF assumes that the model forecast and observations are noisy measurements of the system with some Gaussian errors. The analysis cycle of EnKF relies on the error statistics of the ensemble model forecasts. Let N^e be the ensemble size and $\mathbf{x}$ be the state vector of the dynamical model. The error statistics is calculated using the state vectors $\left(\mathbf{x}_i^b\right), i = 1, \ldots, N^e$ derived from the state variables of each ensemble member. When observations are available, each of the N^e ensemble members are updated according to

$$\mathbf{x}_i^a = \mathbf{x}_i^b + \mathbf{K}\left[\mathbf{y}^o - \mathbf{H}(\mathbf{x}_i^b)\right], \quad 1 \leq i \leq N^e. \tag{6.1}$$

Here, $\mathbf{y}^o$ is a vector of observations, $\mathbf{H}$ is the observation operator which maps model variables to the observations, and $\mathbf{K}$ is the Kalman gain matrix with the form:

$$\mathbf{K} = \mathbf{X}^b\mathbf{Y}^T \left[\frac{1}{N^e - 1}\mathbf{Y}\mathbf{Y}^T + \mathbf{R}\right]^{-1}. \tag{6.2}$$

Notice that we only have one observation available for the model state, which is the zonal wind data obtained from ECMWF. The observation operator in this case is trivial, which is the identity matrix.

The i^{th} column of the matrix $\mathbf{X}^b$ is the difference between each state vector $\mathbf{x}_i^b$ and the background ensemble mean $\overline{\mathbf{x}}^b$. The i^{th} column of the matrix $\mathbf{Y}$ is defined as the difference between each state vector $\mathbf{x}_i^b$ and the ensemble mean after applying the observation operator $\mathbf{H}$ to each state vector. The matrix $\mathbf{R}$ is the observation error covariance matrix. The EnKF is operated in a sequential manner by applying updates, Equation (6.1), at each time when new observations are available. Then, the analysis update will be used as new initial conditions for the next short model forecast and so on.

In this work, the EnKF is used to estimate both the model state as well as the model parameter h, so an augmented state vector is required. As h is assumed to be constant, the simple dynamical model for h is:

$$\frac{dh}{dt} = 0. \tag{6.3}$$

Rewrite the Ruzmaikin model (Equations (5.23-5.25)) in the compact form:

$$\frac{d\mathbf{x}}{dt} = F(t, \mathbf{x}), \tag{6.4}$$

where $\mathbf{x}$ is the l-dimensional model state vector and F defines the vector field. Then the augmented state system is modeled by this four-dimensional dynamical system:

$$\begin{pmatrix} d\mathbf{x}/dt \\ dh/dt \end{pmatrix} = \begin{pmatrix} F(t, \mathbf{x}) \\ 0 \end{pmatrix} = F^*(t, \mathbf{x}^*), \tag{6.5}$$

which is used to generate the background forecast. The analysis is obtained by calculating the error covariance matrices of the augmented state vector and available observations. These two error covariance matrices are used to define the Kalmain gain matrix **K**. The new analysis then will be the initial conditions for the next ensemble forecast and subsequently used to calculated the next analysis cycle and so on. This process is repeated till all the observations of zonal wind are assimilated.

6.3.2 The Ensemble Smoother with Multiple Data Assimilation

The ensemble smoother with multiple data assimilation (ES-MDA) is a global data assimilation method that can be used to solve the history matching problem, which is stated in Chapter 2. In comparison to the sequential data assimilation scheme presented earlier, instead of calculating the analysis step at every time when new observations become available, ES-MDA assimilates the entire time series of the observations at once and generates a global update for uncertain model parameters.

The history matching problem solves a standard inverse problem. First, let us define the history matching problem as:

$$\mathbf{y} = \mathbf{g}(\mathbf{x}). \tag{6.6}$$

Here, $\mathbf{x}$ is the vector of uncertain model parameters including the time-dependent $h(t)$ and initial conditions of the model variables, $\mathbf{y}$ is the predicted measurements of the system (zonal wind field U), and $\mathbf{g}$ is the model operator given by the Ruzmaikin model (Equations (5.23-5.25)). Time series of measurements of the zonal wind are related to the predicted measurements in the form,

$$\mathbf{d} = \mathbf{y} + \epsilon, \tag{6.7}$$

where ϵ is assumed to be the Gaussian observation error with mean of 0.

This inverse problem is formulated using Bayes' theorem (Evensen (2018)), defined as:

$$f(\mathbf{x}|\mathbf{d}) \propto f(\mathbf{d}|\mathbf{g}(\mathbf{x}))f(\mathbf{x}), \tag{6.8}$$

where $f(\mathbf{x}|\mathbf{d})$ is the posterior probability density function (PDF) of the parameters $\mathbf{x}$ conditioned on the observations $\mathbf{d}$. In order to solve this problem, the prior $f(\mathbf{x})$ and the likelihood $f(\mathbf{d}|\mathbf{g}(\mathbf{x}))$ are assumed to be Gaussian distributions. Equation (6.8) is also known as the smoothing problem in data assimilation. Various ensemble smoothing methods have been designed lately to solve this type of problem. Chen and Oliver (2012, 2013) developed the iterative ensemble smoother (IES), which initially was called as ensemble randomized likelihood (EnRML). Emerick and Reynolds (2013) proposed the ensemble smoother with multiple data assimilation (ES-MDA) which is the method adapted here to estimate the time-varying h. In real practice, this data assimilation framework can be used to estimate any uncertain model parameters. In my study, the ES-MDA is used to estimate eight uncertain parameters of the Ruzmaikin model including $h(t)$. In particular, the following parameters are chosen for the vector $\mathbf{x}$:

$$\mathbf{x} = (X_0, Y_0, U_0, \epsilon, \delta\Lambda_a, \Lambda_0, U_R, h(t)), \tag{6.9}$$

where X_0, Y_0, U_0 are initial conditions for the model state vector. The rest of parameters included in the parameter vector are used to define the other control parameter of the model, $\Lambda(t)$. All other model parameters not included in $\mathbf{x}$ are fixed at values defined by Ruzmaikin *et al.* (2003).

The mathematical formulation of the ES-MDA is presented in Chapter 2. Here are the details (followed in the order of steps) of the ensemble framework designed for the Ruzmaikin model:

1. Sample a large prior ensemble of the chosen model parameters including time series of $h(t)$. Each parameter is provided with an initial guess of value and a standard deviation. The prior ensemble for $h(t)$ is provided by the processed ECMWF geopotential height data.

2. Simulate (integrate) the model forward for the entire 20 years (1999 to 2018) using the prior ensemble of uncertain parameters obtained in step 1. This step provides a prior ensemble prediction for the system state which also represents the initial forecast uncertainty.

3. Compute the posterior ensemble of parameters by maximizing a Gaussian likelihood accounting the misfit between the model prediction and observations and the correlations between the input parameters and the predicted measurements.

4. Update the posterior ensemble prediction of the system state with the updated parameters from step 3. The posterior ensemble spread can be used to interpret the uncertainty of posterior model forecasts.

The above algorithm is iterated for a number of steps till the "optimal" model prediction is achieved. The difficulty is to define what an optimal state is, which can be completely different metrics for different applications. In our study, we consider the accuracy of zonal wind speed predictions (in comparison to real observations) as the metric for the computational model performance. In general, one can expect improvements in the model performance as number of iterations increases. However, the computational time/cost can also increase significantly as a result of increasing number of iteration steps. In real practice, a numerical experiment can be done by varying the number of iteration steps and looking for an optimal trade-off between model performance and computational cost. The last iteration's update for

the parameter vector is used to generate the ultimate "optimal" model prediction of a system. In our study, we have found that after 32 steps, the ES-MDA performance does not show remarkable improvement, so we use 32 steps.

6.4 Results and Discussion

6.4.1 Data Assimilation for Time-independent h

The EnKF framework is built for estimating the time-independent h, which follows the same assumption made by Ruzmaikin *et al.* (2003). With the augmented system designed as Equation (6.5), the EnKF can produce an ensemble realizations of constant h. The data processed from ECMWF Reanalysis - Interim are daily means of the zonal wind (corresponds to the model variable U) from 1 January 1999 to 31 December 2018. In order to assimilate the data, the numerical scheme of model simulation is modified accordingly to provide daily means of the zonal wind.

Spin-up of the model (free run of the model) for the initial background ensemble is a common practice in data assimilation. It can provide a representative approximation of the initial uncertainty in model forecasts. In addition to this reason, in the context of the Ruzmaikin model, spin-up is required since the model itself does not align with real seasonality of the reanalysis data, i.e., the model runs do not necessarily start on January 1$^{\text{st}}$, 1999 (or roughly winter time). Therefore, the model is integrated for 500 days before computing the first analysis cycle, which allows the first background ensemble to catch up with the initial seasonality of the data. Though one can always choose a different number of days for spin-up for the same purpose.

In order to generate the spin-up, a suitable choice of the initial ensemble is also required. In Ruzmaikin *et al.* (2003), the initial conditions of model variables X, Y and U are not given. Thus, in our study, we arbitrarily determine the initial values for

each model variable and the parameter h. We manually tune the initial ensemble until desired EnKF results are obtained. The "deseried" result is the one that produces accurate EnKF update for the zonal wind speed in comparison with the ECMWF observations. As the final result of our numerical experiments, reasonable choices for the initial conditions of model variables X and Y for all ensemble members are $X_0 = 0$ and $Y_0 = 0$. The initial value for U is sampled randomly from the range 10 to 100 meters for each ensemble member. The initial value for h is sampled randomly from the range 40 to 120 meters for each ensemble member. Notice that the chosen ranges for U and h are also within the bistable region shown in Figure 5.1.

Furthermore, there are other algorithmic parameters such as the observation error, inflation factor, and ensemble size that could be varied to optimize EnKF's performance. In Figure 6.2, the settings for the algorithmic parameters are: observation error (observation variance) of 0.1, no inflation (inflation factor of 1), and 1000 ensemble members. This plot of zonal wind speed produced by EnKF algorithm shows that though the ensemble mean (maroon line) agrees well with the seasonal pattern of the ECMWF data (dark connected dots), the mean does not reproduce the bistability of the wind observed in the data. For example, the peaks of the ensemble mean (wintertime zonal flow speed) always converge to the slower winter wind observed in the data. Nevertheless, the ensemble members (gray lines) in the same plot demonstrate spread of zonal wind every winter with some ensemble members converging to the faster winter wind. Hence, the bistability behavior is found in the ensemble members but not present in the ensemble mean of zonal flow. Moreover, Figure 6.3 shows the corresponding update for h under the same EnKF experiment. The ensemble mean of h (green line) settles around 80 meters after 2008, which is within the bistable region shown in Figure 5.1.

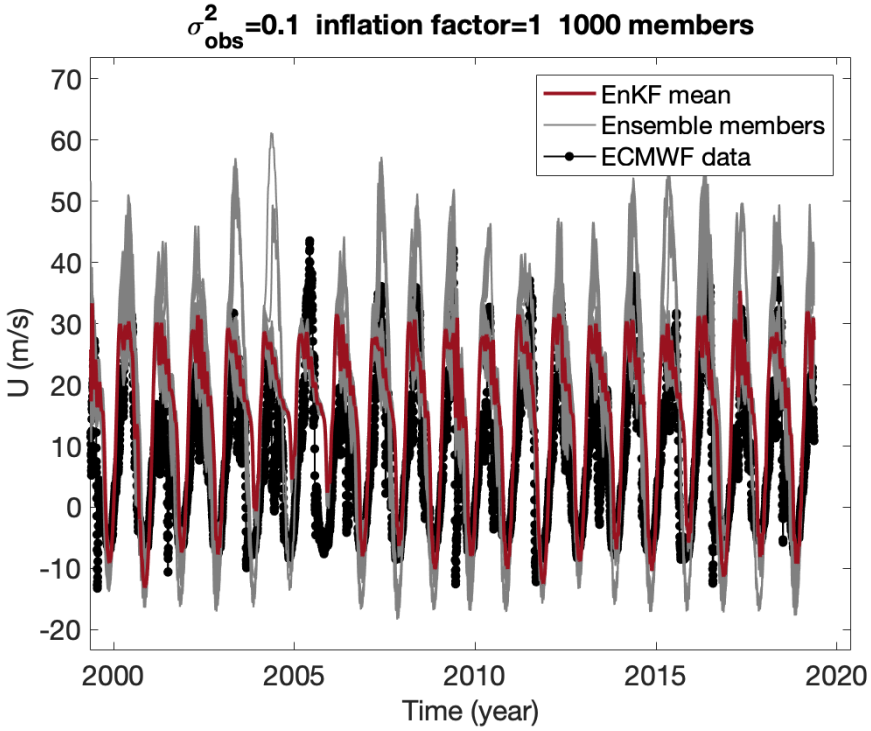

Figure 6.2: The EnKF update for zonal wind speed U after assimilating the corresponding ECMWF observations. The ensemble is initialized with 1000 ensemble members which are plotted in gray. The ensemble mean is plotted in maroon and observations are plotted as black dots. The ensemble forecasts run from 1999 to 2018.

Figures 6.4 and 6.5 illustrate the result of another numerical experiment in which a much smaller observation error of 0.001 and a inflation factor of 1.02 are chosen. The inflation factor is used to account for model errors. The EnKF update of U shown in Figures 6.4 shows that both the ensemble mean and the ensemble members capture the bistability behavior of the zonal wind observed in data. However, the update of h shown in Figures 6.5 settles at 0 meter after year 2004, which implies that there is no planetary waves. In this case, the EnKF has given priority to trust the data due to a very small observation error, so it may ignore the background forecast. As a

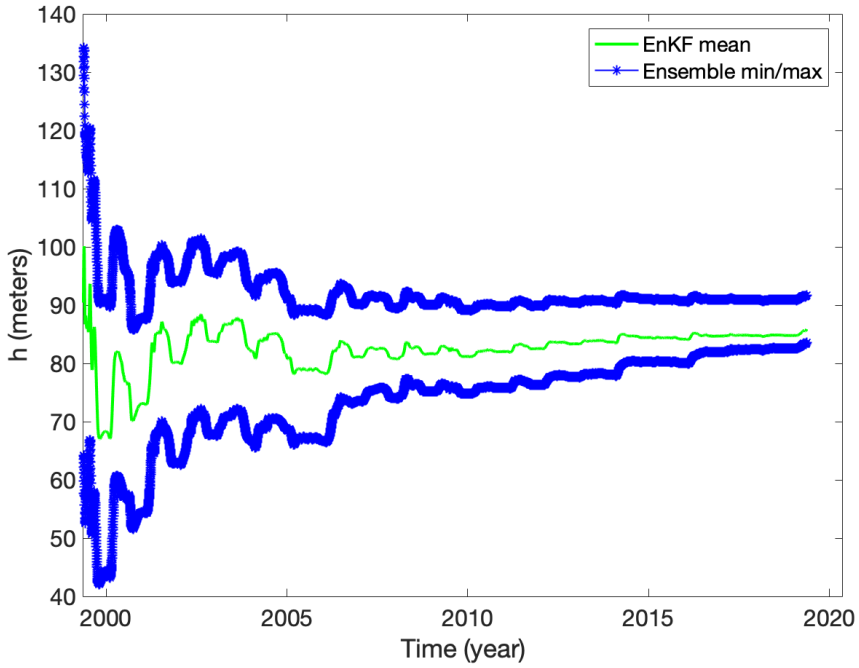

Figure 6.3: The EnKF update for h corresponding to the update of U in Figure 6.2. Ensemble mean of h is plotted in green and minimum and maximum values of ensemble are in blue.

result, the EnKF updates for U and h show that the Ruzmaikin model is unable to explain the observed dynamics in data with the bifurcation analysis of h.

Although these two model runs of the EnKF reproduce the seasonal pattern of the data (annual variation of the jet) in the update of U, the results produced under the model assumption that h is constant are limited to explain the bistability behavior (inter-annual variation) of the zonal wind seen in the data.

6.4.2 Data Assimilation for Time-varying h

The ES-MDA is used here to explore the alternative assumption that h is time-dependent. Unlike the EnKF where both the state variables X, Y, and U and the

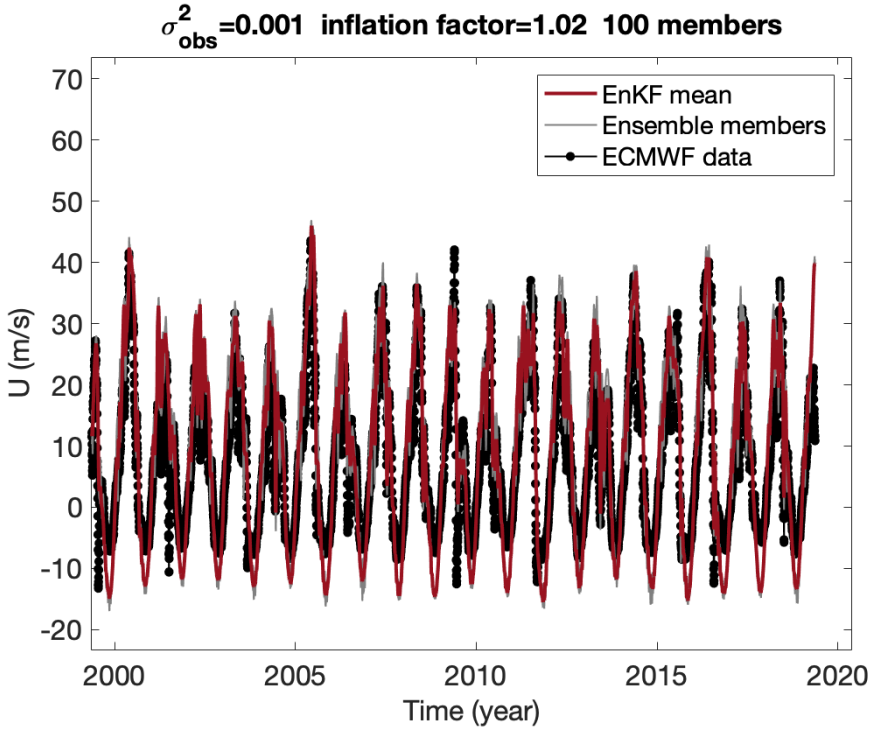

Figure 6.4: The EnKF update for U (m/s) with 100 ensemble members and a much smaller observation error. The ensemble mean (in maroon) is plotted together with each ensemble member (in gray) and observations (black dots). The gray lines of ensemble members all converge to the data throughout the 20 years, so we do not observe the spread in ensemble members.

model parameter h are updated together, the ES-MDA updates only the parameter space. In particular, eight uncertain model parameters are chosen to be estimated. The parameter vector is defined as $\mathbf{x} = (X_0, Y_0, U_0, \epsilon, \delta\Lambda_a, \Lambda_0, U_R, h(t))$. The rest of the model parameters are fixed throughout the model runs.

The geopotential height data obtained from ECMWF reanalysis are used to provide a prior ensemble for the time-varying $h(t)$, which provides $\sim$ 7300 days (20 years) of data. Moreover, the 500-day spin-up is also applied here so that the background ensemble resembles the seasonality of data. Consequently, the dimension of $h(t)$ con-

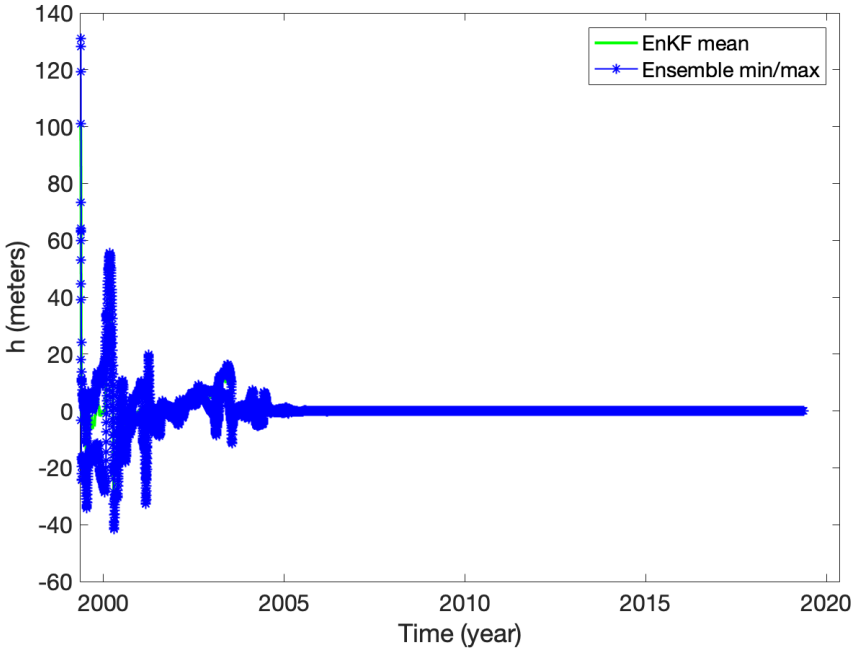

Figure 6.5: The EnKF update for h corresponding to the update for U in Figure 6.4. Ensemble mean and extreme values of h are plotted. The green line of the mean seems to disappear as it is overlaid by the blue curves of extreme values.

sists of archived output during a spin-up time period and analyzed times with a total dimension of ~ 7800. At each ES-MDA step, the twenty years of zonal wind observations are assimilated all at once to update the chosen parameter space including time series of $h(t)$. The ES-MDA is iterated 32 times to provide the final output for $h(t)$ and other chosen model parameters. The final updated parameters are used to integrate the model forward for 20 years to provide the "optimal" model prediction. The performance of the algorithm is assessed by the accuracy of predictions for the zonal wind speed U in comparison to the data.

Figure 6.6 presents a representative result from the ES-MDA algorithm. The top and bottom panels are ensemble realizations (with 1000 ensemble members) for U and

$h(t)$, respectively. The posterior ensemble mean of U produced at the last ES-MDA step (orange curve) recovers the bistability behavior seen in the data. Moreover, such update of U corresponds to the bottom panel of time-dependent h, which shows regular oscillations between strong and weak tropospheric forcing from planetary waves throughout the 20 years. When slower winter zonal flow is observed between year 2001 and year 2004, the posterior ensemble mean of $h(t)$ (dark green curve) shows rapid increase with a huge spike right after year 2000. This combination of small U and large h resembles the lower stable branch (unstable polar vortex) of the bifurcation diagram seen as in Figure 5.1. (Here we are looking at the qualitative behaviors of the forecasts instead of quantitative results.) Similarly, when fast winter zonal wind is observed in the data, such as the year 2005 or 2016, the ES-MDA produces an update of smaller h in the posterior, which implies less perturbation from planetary waves to the polar jet. This combination of large U and small h maps to the upper branch (stable polar vortex) of the bifurcation diagram of h. The ES-MDA update of $h(t)$ verifies the qualitative behavior of inter-annual variation of the system studied by the Ruzmaikin model.

The prior ensemble of time-dependent h at the first iteration of the ES-MDA is obtained from the analyzed ECMWF geopotential height data as described in Section 6.2.2. In Figure 6.6, this prior ensemble of $h(t)$ (light blue lines) converge to the posterior mean of $h(t)$ (dark green line) after the last iteration of the ES-MDA. The final predicted ensemble mean of $h(t)$ suggests much stronger forcing from planetary waves than what is observed from the reanalysis data during wintertime. This comparison between the prior and posterior of $h(t)$ confirms that h plays an important role to recover the observed dynamics of zonal wind.

However, there are also a small number of updates of h that are not consistent with the bifurcation analysis in Ruzmaikin *et al.* (2003). For example, a fast winter

zonal flow is observed in year 2012, but it corresponds to a large h update from the ES-MDA, which disagrees with the bifurcation analysis that a strong planetary wave forcing is associated with a weak polar jet and an unstable polar vortex. There is an inherent model bias because of the simplified dynamics and physics in the model employed. Not all the observed stratospheric dynamics can be explained using this idealized model.

The Ruzmaikin model is a mechanistic model developed to study the underlying mechanisms of the observed dynamics of the Arctic polar vortex. Under the assumption that h is time-dependent, the prediction given by the ES-MDA recovers more interesting dynamics than the prediction obtained by the EnKF for time-independent h. The bistability of the wind associated with change in h is also validated by the ES-MDA updates for U and h. Although the Ruzmaikin model is a reduced-order model that simplifies the complex high-dimensional system of the polar vortex, it can reproduce the qualitative patterns of the observed dynamics of polar vortex and provide insights of underlying mechanism with its bifurcation analysis of h.

6.5 Conclusions

A reduced-order model developed by Ruzmaikin *et al.* (2003) can be used to study the underlying mechanisms of stratospheric polar vortex in the Northern Hemisphere. In particular, two important model parameters are used to understand the stratospheric response to perturbations from solar forcing and planetary waves. These two parameters are: the vertical gradient of the zonal wind, Λ, and the initial amplitude of planetary waves, h.

Although the idealized model cannot be used to predict or reproduce the high-dimensional system of the polar vortex, it provides insightful explanations for the qualitative behaviors of such a complex dynamical system. In particular, the bi-

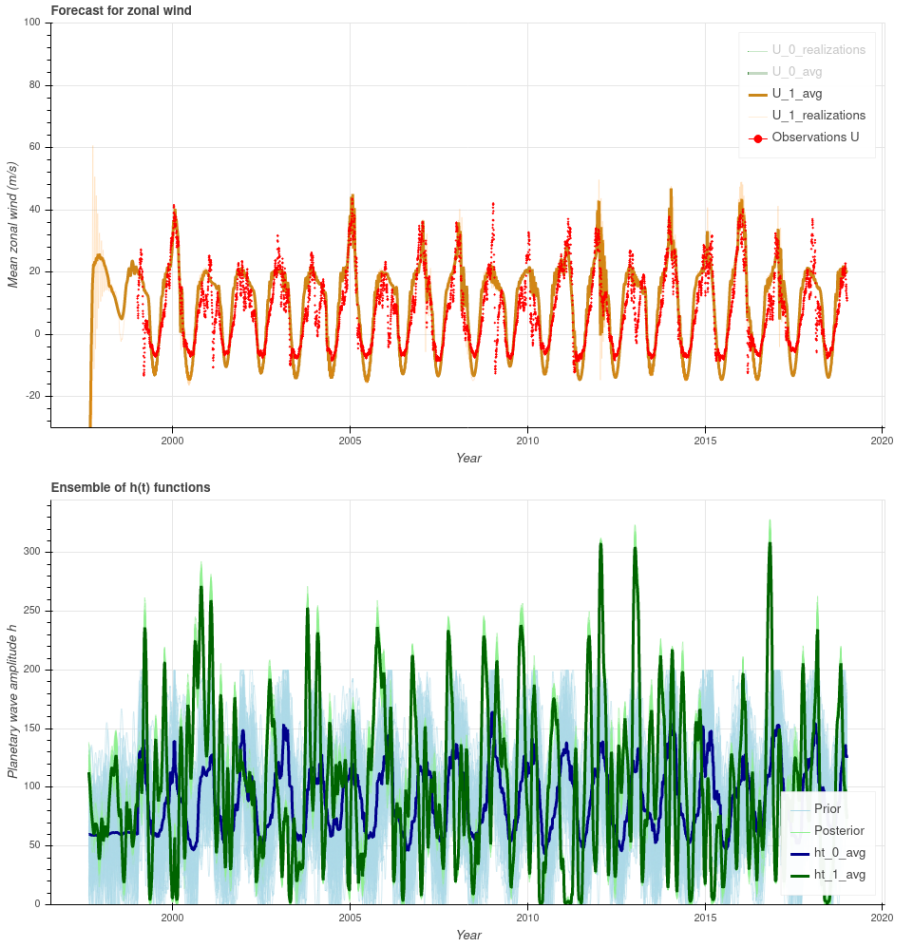

Figure 6.6: ES-MDA updates for U and time-dependent h. **Top**: ensemble forecast for zonal wind U (m/s). The ensemble mean is in orange, and ensemble members are in lighter orange but all converge to the mean after spin up. The red points are ECMWF data. **Bottom**: posterior and prior ensembles of $h(t)$.The mean of prior is in dark blue and the mean of posterior is in dark green. The lighter blue and lighter green are ensemble members of prior and posterior respectively.

furcation analysis of h suggests the inter-annual variability of the polar vortex in connection with forcing from planetary waves, which can be seen through modulation of the number of cold and warm winters. A fair question to ask based on the analysis of the model is: are these modeled qualitative behaviors also observed in real data? Assessment and validation of the idealized model is required to answer this question.

Two different data assimilation methods are used in my study in order to assess the model. The first approach is a sequential data assimilation scheme called the ensemble Kalman filter (EnKF), which is used to test the assumption that h is time-independent. The other approach is a global data assimilation scheme called the ensemble smoother with multiple data assimilation (ES-MDA), which is used to test the assumption that h is time-dependent. Both methods provides estimates for the parameter h using the same data set post-processed from the ECMWF Reanalysis - Interim archive.

The qualitative behaviors of the model are reproduced (validated) in the data assimilation results. The EnKF ensemble prediction of the zonal wind U (Figure 6.2) reproduces the seasonal pattern of the wind data. Additionally, the bistability behavior is observed in the spread of ensemble members, although the ensemble mean does not show bistability. The corresponding h update (Figure 6.3) also lies within the bistability region seen as in Figure 5.1. To reproduce the bistability in the ensemble mean, a much smaller observation error is applied for the EnKF algorithm (Figures 6.4 and 6.5). However, in this case the model is not meaningful to interpret the results as the EnKF update for h converged to 0 meter which is not physical.

The assumption of a time-varying h is more representative of the real dynamics. The ES-MDA framework is able to estimate the time series of h. Corresponding results show large variability in h in the posterior prediction of the parameter (Figure

6.6). Moreover, the bistabilty behavior of the zonal flow is reproduced well with such time-dependent h. The two stable steady states in the bifurcation diagram of h are realized in the posterior updates for h and U qualitatively, which supports the model's analysis. A stable polar vortex is associated with less perturbation from planetary waves (upper branch in Figure 5.1), and an unstable polar vortex is associated with larger perturbation from planetary waves (lower branch in Figure 5.1).

Data assimilation is a useful tool to diagnose model biases for reduced-order models. Two different data assimilation frameworks are used to test different assumptions of the model: h is time-dependent or time-independent. Assimilating data produced by a global forecast model reveals deficiency in the low-dimensional model. The assumption of a constant h (steady forcing from planetary waves) is not realistic to recover the bistability pattern observed in the data, whereas a time-varying h is capable. Model assumptions can be tested via suitable data assimilation methods, which can aid with better model development.

Aanonsen, S. I., G. Nævdal, D. S. Oliver, A. C. Reynolds and B. Vallès, "The ensemble kalman filter in reservoir engineering–a review", Spe Journal **14**, 03, 393–412 (2009).

ACS, "Key statistics for prostate cancer: Prostate cancer facts", `https://www.cancer.org/cancer/prostate-cancer/about/key-statistics.html`, (Accessed: 05 October 2021) (2021).

Anderson, J. L., "An ensemble adjustment kalman filter for data assimilation", Monthly weather review **129**, 12, 2884–2903 (2001).

Anderson, J. L. and S. L. Anderson, "A monte carlo implementation of the nonlinear filtering problem to produce ensemble assimilations and forecasts", Monthly weather review **127**, 12, 2741–2758 (1999).

Arnold, Jr., C. P. and C. H. Day, "Observing-systems simulation experiments: Past, present, and future", Bulletin of the American Meteorological Society **67**, 6, 687–695 (1986).

Baek, S. J., B. R. Hunt, E. Kalnay, E. Ott and I. Szunyogh, "Local ensemble Kalman filtering in the presence of model bias", Tellus A **58**, 3, 293–306 (2006).

Baez, J. and Y. Kuang, "Mathematical models of androgen resistance in prostate cancer patients under intermittent androgen suppression therapy", Applied Sciences **6**, 11, 352 (2016).

Balachandran, N. K., D. Rind, P. Lonergan and D. T. Shindell, "Effects of solar cycle variability on the lower stratosphere and the troposphere", J. Geophys. Res. **104**, 27321–27339 (1999).

Barnes, S. L., "A technique for maximizing details in numerical weather map analysis", Journal of Applied Meteorology and Climatology **3**, 4, 396–409 (1964).

Bengtsson, L., M. Ghil and E. Källén, *Dynamic meteorology: data assimilation methods*, vol. 36 (Springer, 1981).

Bergthörsson, P. and B. R. Döös, "Numerical weather map analysis", Tellus **7**, 3, 329–340 (1955).

Berrisford, P., D. Dee, P. Poli, R. Brugge, K. Fielding, M. Fuentes, P. Kållberg, S. Kobayashi, S. Uppala and A. Simmons, "The era-interim archive version 2.0, shinfield park", Reading **1**, 23 (2011).

Box, G. E., "Science and statistics", Journal of the American Statistical Association **71**, 356, 791–799 (1976).

Bruchovsky, N., L. Klotz, J. Crook, S. Malone, C. Ludgate, W. J. Morris, M. E. Gleave and S. L. Goldenberg, "Final results of the Canadian prospective Phase II trial of intermittent androgen suppression for men in biochemical recurrence after radiotherapy for locally advanced prostate cancer: Clinical parameters", Cancer **107**, 2, 389–395 (2006).

Burgers, G., P. Jan van Leeuwen and G. Evensen, "Analysis scheme in the ensemble kalman filter", Monthly weather review **126**, 6, 1719–1724 (1998).

Carrassi, A., M. Bocquet, L. Bertino and G. Evensen, "Data assimilation in the geosciences: An overview of methods, issues, and perspectives", Wiley Interdisciplinary Reviews: Climate Change **9**, 5, e535 (2018).

Ch, H. and C. Hodges, "The effect of castration, of estro gen and of androgen injection on serum phosphatases in metastatic carcinoma of the prostate", Cancer research (1941).

Charney, J. G., "Dynamic forecasting by numerical process", in "Compendium of meteorology", pp. 470–482 (Springer, 1951).

Chen, Y. and D. S. Oliver, "Ensemble randomized maximum likelihood method as an iterative ensemble smoother", Mathematical Geosciences **44**, 1, 1–26 (2012).

Chen, Y. and D. S. Oliver, "Levenberg–marquardt forms of the iterative ensemble smoother for efficient history matching and uncertainty quantification", Computational Geosciences **17**, 4, 689–703 (2013).

Cressman, G. P., "An operational objective analysis system", Monthly Weather Review **87**, 10, 367–374 (1959).

Daley, R., *Atmospheric data analysis*, no. 2 (Cambridge university press, 1993).

Droop, M. R., "Vitamin b12 and marine ecology. iv. the kinetics of uptake, growth and inhibition in monochrysis lutheri", Journal of the Marine Biological Association of the United Kingdom **48**, 3, 689–733 (1968).

Eisenberg, M. C. and M. A. L. Hayashi, "Determining identifiable parameter combinations using subset profiling", Mathematical Biosciences **256**, 116–126, URL `http://linkinghub.elsevier.com/retrieve/pii/S0025556414001631` (2014).

Eisenberg, M. C. and H. V. Jain, "A confidence building exercise in data and identifiability: Modeling cancer chemotherapy as a case study", Journal of Theoretical Biology **431**, 63–78 (2017).

Emerick, A. A. and A. C. Reynolds, "Ensemble smoother with multiple data assimilation", Computers & Geosciences **55**, 3–15 (2013).

Errico, R. M., R. Yang, N. C. Privé, K.-S. Tai, R. Todling, M. E. Sienkiewicz and J. Guo, "Development and validation of observing-system simulation experiments at NASAs Global Modeling and Assimilation Office", Quarterly Journal of the Royal Meteorological Society A **139**, 1162–1178 (2013).

Evensen, G., "Sequential data assimilation with a nonlinear quasi-geostrophic model using Monte Carlo methods to forecast error statistics", Journal of Geophysical Research: Oceans **99**, C5, 10143–10162 (1994).

Evensen, G., "The ensemble Kalman filter: Theoretical formulation and practical implementation", Ocean Dynamics **53**, 4, 343–367 (2003).

Evensen, G., "Sampling strategies and square root analysis schemes for the enkf", Ocean dynamics **54**, 6, 539–560 (2004).

Evensen, G., *Data assimilation: the ensemble Kalman filter* (Springer Science & Business Media, 2009a).

Evensen, G., "The ensemble kalman filter for combined state and parameter estimation", IEEE Control Systems Magazine **29**, 3, 83–104 (2009b).

Evensen, G., "Analysis of iterative ensemble smoothers for solving inverse problems", Computational Geosciences **22**, 3, 885–908 (2018).

Evensen, G., J. Amezcua and et. al, "An international initiative of predicting the sars-cov-2 pandemic using ensemble data assimilation", Foundations of Data Science **0**, – (2020).

Evensen, G. and P. J. Van Leeuwen, "An ensemble kalman smoother for nonlinear dynamics", Monthly Weather Review **128**, 6, 1852–1867 (2000).

Feldman, B. J. and D. Feldman, "The development of androgen-independent prostate cancer", Nature Reviews Cancer **1**, 1, 34–45 (2001).

Geisler, J., "A numerical model of the sudden stratospheric warming mechanism", Journal of Geophysical Research **79**, 33, 4989–4999 (1974).

Ghil, M. and P. Malanotte-Rizzoli, "Data assimilation in meteorology and oceanography", Advances in geophysics **33**, 141–266 (1991).

Hamill, T. M., J. S. Whitaker and C. Snyder, "Distance-dependent filtering of background error covariance estimates in an ensemble kalman filter", Monthly Weather Review **129**, 11, 2776–2790 (2001).

Hirata, Y., N. Bruchovsky and K. Aihara, "Development of a mathematical model that predicts the outcome of hormone therapy for prostate cancer", Journal of Theoretical Biology **264**, 2, 517–527, URL `http://dx.doi.org/10.1016/j.jtbi.2010.02.027` (2010).

Hoke, J. E. and R. A. Anthes, "The initialization of numerical models by a dynamic-initialization technique", Monthly Weather Review **104**, 12, 1551–1556 (1976).

Holton, J. R. and T. Dunkerton, "On the role of wave transience and dissipation in stratospheric mean flow vacillations", Journal of Atmospheric Sciences **35**, 4, 740–744 (1978).

Holton, J. R. and C. Mass, "Stratospheric vacillation cycles", Journal of Atmospheric Sciences **33**, 11, 2218–2225 (1976).

Houtekamer, P. L. and H. L. Mitchell, "Data assimilation using an ensemble kalman filter technique", Monthly Weather Review **126**, 3, 796–811 (1998).

Houtekamer, P. L. and F. Zhang, "Review of the ensemble kalman filter for atmospheric data assimilation", Monthly Weather Review **144**, 12, 4489–4532 (2016).

Hu, Y. and K. K. Tung, "Interannual and decadal variations of planetary wave activity, stratospheric cooling, and northern hemisphere annular mode", Journal of Climate **15**, 13, 1659–1673 (2002).

Hunt, B. R., E. J. Kostelich and I. Szunyogh, "Efficient data assimilation for spatiotemporal chaos: A local ensemble transform Kalman filter", Physica D **230**, 1–2, 112–126 (2007).

Ideta, A. M., G. Tanaka, T. Takeuchi and K. Aihara, "A mathematical model of intermittent androgen suppression for prostate cancer", Journal of nonlinear science **18**, 6, 593–614 (2008).

Kalman, R. E., "A new approach to linear filtering and prediction problems", (1960).

Kalman, R. E. and R. S. Bucy, "New results in linear filtering and prediction theory", (1961).

Kalnay, E., *Atmospheric modeling, data assimilation and predictability* (Cambridge university press, 2003).

Kistler, R. E., *A study of data assimilation techniques in an autobarotropic, primitive equation, channel model*, Ph.D. thesis, Pennsylvania State University (1974).

Kostelich, E., "Symphony in chaos", New Scientist-UK Edition **146**, 1972, 36–39 (1995).

Kumar, S., M. Shelley, C. Harrison, B. Coles, T. J. Wilt and M. Mason, "Neo-adjuvant and adjuvant hormone therapy for localised and locally advanced prostate cancer", Cochrane Database of Systematic Reviews , 4 (2006).

Lorenz, E. N., "A study of the predictability of a 28-variable atmospheric model", Tellus **17**, 3, 321–333 (1965).

Miao, H., X. Xia, A. S. Perelson and H. Wu, "On identifiability of nonlinear ODE models and applications in viral dynamics", SIAM Review **53**, 1, 3–39 (2011).

Neal, R. M., "Sampling from multimodal distributions using tempered transitions", Statistics and computing **6**, 4, 353–366 (1996).

Ott, E., B. R. Hunt, I. Szunyogh, M. Corazza, E. Kalnay, D. Patil, J. A. Yorke, A. V. Zimin and E. J. Kostelich, "Exploiting local low dimensionality of the atmospheric dynamics for efficient ensemble kalman filtering", arXiv preprint physics/0203058 **3** (2002).

Ott, E., B. R. Hunt, I. Szunyogh, A. V. Zimin, E. J. Kostelich, M. Corazza, E. Kalnay, D. Patil and J. A. Yorke, "A local ensemble kalman filter for atmospheric data assimilation", Tellus A: Dynamic Meteorology and Oceanography **56**, 5, 415–428 (2004).

Phan, T., S. M. Crook, A. H. Bryce, C. C. Maley, E. J. Kostelich and Y. Kuang, "Mathematical modeling of prostate cancer and clinical application", Applied Sciences **10**, 8, 2721 (2020).

Phan, T., K. Nguyen, P. Sharma and Y. Kuang, "The impact of intermittent androgen suppression therapy in prostate cancer modeling", Applied Sciences **9**, 1, 36 (2019).

Portz, T., Y. Kuang and J. D. Nagy, "A clinical data validated mathematical model of prostate cancer growth under intermittent androgen suppression therapy", AIP Advances **2**, 1, 0–14, URL `http://scitation.aip.org/content/aip/journal/adva/2/1/10.1063/1.3697848` (2012).

Raue, A., C. Kreutz, T. Maiwald, J. Bachmann, M. Schilling, U. Klingmüller and J. Timmer, "Structural and practical identifiability analysis of partially observed dynamical models by exploiting the profile likelihood", Bioinformatics **25**, 15, 1923–1929 (2009).

Ruzmaikin, A., J. Lawrence and C. Cadavid, "A simple model of stratospheric dynamics including solar variability", Journal of climate **16**, 10, 1593–1600 (2003).

Sasaki, Y., "Some basic formalisms in numerical variational analysis", Monthly Weather Review **98**, 12, 875–883 (1970).

Skjervheim, J.-A., G. Evensen, J. Hove, J. G. Vabø *et al.*, "An ensemble smoother for assisted history matching", in "SPE Reservoir Simulation Symposium", (OnePetro, 2011).

Spry, N. A., L. Kristjanson, B. Hooton, L. Hayden, H. Neerhut, G. an Gurney, T. Corica, E. Korbel, S. Weinstein and K. McCaul, "Adverse effects to quality of life arising from treatment can recover with intermittent androgen suppression in men with prostate cancer", European Journal of Cancer **42**, 1083–1092 (2006).

Stordal, A. S. and A. H. Elsheikh, "Iterative ensemble smoothers in the annealed importance sampling framework", Advances in Water Resources **86**, 231–239 (2015).

Talagrand, O., "Assimilation of observations, an introduction (gtspecial issueltdata assimilation in meteology and oceanography: Theory and practice)", Journal of the Meteorological Society of Japan. Ser. II **75**, 1B, 191–209 (1997).

Tippett, M. K., J. L. Anderson, C. H. Bishop, T. M. Hamill and J. S. Whitaker, "Ensemble square root filters", Monthly Weather Review **131**, 7, 1485–1490 (2003).

Whitaker, J. S. and T. M. Hamill, "Ensemble data assimilation without perturbed observations", Monthly weather review **130**, 7, 1913–1924 (2002).

Wu, Z., T. Phan, J. Baez, Y. Kuang and E. J. Kostelich, "Predictability and identifiability assessment of models for prostate cancer under androgen suppression therapy", Mathematical Biosciences and Engineering **16**, 5, 3512–3536 (2019).

Yoden, S., "Bifurcation properties of a stratospheric vacillation model", Journal of the atmospheric sciences **44**, 13, 1723–1733 (1987).

Yoden, S., "An illustrative model of seasonal and interannual variations of the stratospheric circulation", Journal of the atmospheric sciences **47**, 15, 1845–1853 (1990).

Yorke, E., Z. Fuks, L. Norton, W. Whitmore and C. Ling, "Modeling the development of metastases from primary and locally recurrent tumors: comparison with a clinical data base for prostatic cancer", Cancer research **53**, 13, 2987–2993 (1993).

APPENDIX A

JOURNAL PERMISSION

Some of the material in Chapter 3 and 4 was published in Wu *et al.* (2019) and Phan *et al.* (2019), which are given permission to reuse under an open access Creative Common CC BY license.

A figure from Ruzmaikin *et al.* (2003) is reused in Chapter 5, which is given the written permission by the copyright holder: "You may include Figure 3 from Ruzmaikin, Lawrence, and Cadavid's 2003 JCLI article in your ASU thesis, Data Assimilation and Uncertainty Quantification with Reduced-Order Models, with the following conditions:

1. Include the complete bibliographic citation of the original source.
2. Include the following statement with that citation: © American Meteorological Society. Used with permission."

APPENDIX B

CODE ACCESS

The code of the data assimilation applications developed for Chapter 4 and 6 are available to the public on the GitHub repository `https://github.com/zhiminwu29`.